Solar Phys (2017) 292:64
DOI 10.1007/s11207-017-1091-6

The Interaction of Successive Coronal Mass Ejections: A Review

Noé Lugaz[1] · Manuela Temmer[2] · Yuming Wang[3] · Charles J. Farrugia[1]

Received: 15 September 2016 / Accepted: 3 April 2017

Abstract We present a review of the different aspects associated with the interaction of successive coronal mass ejections (CMEs) in the corona and inner heliosphere, focusing on the initiation of series of CMEs, their interaction in the heliosphere, the particle acceleration associated with successive CMEs, and the effect of compound events on Earth's magnetosphere. The two main mechanisms resulting in the eruption of series of CMEs are sympathetic eruptions, when one eruption triggers another, and homologous eruptions, when a series of similar eruptions originates from one active region. CME – CME interaction may also be associated with two unrelated eruptions. The interaction of successive CMEs has been observed remotely in coronagraphs (with the *Large Angle and Spectrometric Coronagraph Experiment* – LASCO – since the early 2000s) and heliospheric imagers (since the late 2000s), and inferred from *in situ* measurements, starting with early measurements in the 1970s. The interaction of two or more CMEs is associated with complex phenomena, including magnetic reconnection, momentum exchange, the propagation of a fast magnetosonic shock through a magnetic ejecta, and changes in the CME expansion. The presence of a preceding CME a few hours before a fast eruption has been found to be

Earth-affecting Solar Transients
Guest Editors: Jie Zhang, Xochitl Blanco-Cano, Nariaki Nitta, and Nandita Srivastava

✉ N. Lugaz
noe.lugaz@unh.edu

M. Temmer
manuela.temmer@uni-graz.at

Y. Wang
ymwang@ustc.edu.cn

C.J. Farrugia
charlie.farrugia@unh.edu

1 Space Science Center and Department of Physics, University of New Hampshire, Durham, NH, USA

2 Institute of Physics, University of Graz, Universitätsplatz 5, 8010 Graz, Austria

3 School of Earth and Space Sciences, University of Science and Technology of China, Hefei 230026, China

Published online: 10 April 2017

connected with higher fluxes of solar energetic particles (SEPs), while CME – CME interaction occurring in the corona is often associated with unusual radio bursts, indicating electron acceleration. Higher suprathermal population, enhanced turbulence and wave activity, stronger shocks, and shock – shock or shock – CME interaction have been proposed as potential physical mechanisms to explain the observed associated SEP events. When measured *in situ*, CME – CME interaction may be associated with relatively well organized multiple-magnetic cloud events, instances of shocks propagating through a previous magnetic ejecta or more complex ejecta, when the characteristics of the individual eruptions cannot be easily distinguished. CME – CME interaction is associated with some of the most intense recorded geomagnetic storms. The compression of a CME by another and the propagation of a shock inside a magnetic ejecta can lead to extreme values of the southward magnetic field component, sometimes associated with high values of the dynamic pressure. This can result in intense geomagnetic storms, but can also trigger substorms and large earthward motions of the magnetopause, potentially associated with changes in the outer radiation belts. Future *in situ* measurements in the inner heliosphere by *Solar Probe+* and *Solar Orbiter* may shed light on the evolution of CMEs as they interact, by providing opportunities for conjunction and evolutionary studies.

Keywords Coronal mass ejections · CME initiation · CME interaction · Solar energetic particles · Solar-terrestrial relations · Radio emission · Geoeffects

1. Introduction

Understanding coronal mass ejections (CMEs) is central to better grasp the complexities of the heliosphere because together with flares, they represent the most intense phenomena in the Sun – Earth system. At the Sun, the exact cause(s) and trigger(s) of CME initiation are still a matter of debate (see review by Chen, 2011), but it is well established that CMEs are one of the main ways for currents and magnetic energy to be released. CMEs typically consist of mostly closed magnetic field lines and carry mass and magnetic flux into the interplanetary (IP) space. Therefore, during times of high solar activity, CMEs highly structure the solar wind plasma and interplanetary magnetic field (IMF) characteristics in the IP space.

CMEs play an important role in the heliospheric magnetic flux balance by dragging magnetic field lines through the Alfvén surface (Owens and Crooker, 2006; Schwadron, Connick, and Smith, 2010). CME-driven shocks are overwhelmingly thought to be the main accelerator of gradual solar energetic particles (SEPs) (Kahler *et al.*, 1984; Reames, 2013). CMEs are also the primary drivers of intense geomagnetic storms at Earth (Gonzalez and Tsurutani, 1987; Gosling *et al.*, 1991; Webb *et al.*, 2000; Zhang *et al.*, 2007), and they are also associated with many of the strongest substorms (Kamide *et al.*, 1998; Tsurutani *et al.*, 2015), changes in Earth radiation belts (Miyoshi and Kataoka, 2005), and geomagnetically induced currents (GICs) (Huttunen *et al.*, 2008). A recent review of CME research can be found in Gopalswamy (2016).

The rate of CMEs during the solar cycle is highly variable, ranging at the Sun from 2 – 3 CMEs *per* week in solar minimum to 5 – 6 CMEs *per* day in solar maximum. Some CME properties in the corona are now routinely measured by space-based coronagraphs such as the *Large Angle and Spectrometric Coronagraph Experiment* onboard the *Solar and Heliospheric Observatory* (SOHO/LASCO: Domingo, Fleck, and Poland, 1995; Brueckner *et al.*, 1995) and the *Solar-Terrestrial Relations Observatory* coronagraphs

(STEREO/COR: Kaiser *et al.*, 2008). Catalogs such as the Coordinated Data Analysis Workshops (CDAW) CME catalog (Yashiro, Michalek, and Gopalswamy, 2008; Gopalswamy *et al.*, 2009) report the CME speed, mass, acceleration, and angular width projected onto the plane-of-the-sky of the instruments. New catalogs such as the Heliospheric Cataloguing, Analysis and Techniques Service (HELCATS)[1] based on STEREO/*Heliospheric Imager* (HI: Eyles *et al.*, 2009) observations give CME speed and direction in the IP space. CME properties near Earth are directly measured by spacecraft such as the *Advanced Composition Explorer* (ACE), *Wind*, or the *Deep Space Climate Observatory* (DSCOVR, operational since 27 July 2016). CME properties may be strongly influenced by their interaction with the solar wind and IMF. To first order, this interaction results in a deceleration of fast CMEs and an acceleration of slow CMEs (Gopalswamy *et al.*, 2000; Vršnak, 2001; Cargill, 2004; Liu *et al.*, 2013), changes in the radial expansion rate of the magnetic ejecta (Gulisano *et al.*, 2010; Poomvises, Zhang, and Olmedo, 2010), and sometimes, its deflection (Wang *et al.*, 2014b) and rotation (Nieves-Chinchilla *et al.*, 2012). Adding to these broad tendencies, CME properties may change even more drastically when they interact with corotating solar wind structures, such as fast wind streams and corotating interaction regions (CIRs) and with other CMEs. The interaction of a CME with a CIR has been studied both through numerical modeling and data analysis (Prise *et al.*, 2015; Winslow *et al.*, 2016).

Combining the CME frequency and their typical propagation times (3 – 4 days from Sun to Earth), there may be as few as two CMEs or as many as 20 in the 4π sr between the Sun and the Earth, depending on the phase of the solar cycle. Assuming that a CME and its shock wave can be modeled as a cone of 30° half-angle, a CME occupies approximately $\pi/4$ sr. During solar maximum, interaction between unrelated successive CMEs is bound to occur; however, CME – CME interaction also occurs regularly even in more quiet phases of the solar cycle. Solar observations often reveal that recurrent CMEs occur from the same active region, often associated with homologous flares (Schmieder *et al.*, 1984; Svestka *et al.*, 1989). On the other hand, sympathetic flares and CMEs may be an even more frequent cause of successive CMEs in relatively close angular and temporal separation (*i.e.* in optimal conditions for at least partial interaction). Early work based on coronagraphic observations (Hansen *et al.*, 1974) and simulations (Steinolfson, 1982) discussed the possibility and consequences of successive quasi-homologous eruptions on the corona.

During their propagation from Sun to Earth, the interaction of successive CMEs may take a variety of forms: 1) the two CME-driven shock waves may interact without the ejecta interacting, 2) one shock wave may interact with a preceding magnetic ejecta, or 3) the successive magnetic ejecta may interact and/or reconnect. The fact that CMEs can interact on their way to Earth has been known for several decades. Some of the early articles focused on the series of seven flares in 72 hours in early August 1972 and the associated three or four shock waves measured by *Pioneer 9*, *Prognoz,* and the *the Interplanetary Monitoring Platform-5* (IPM-5) in the inner heliosphere and one shock wave measured by *Pioneer 10* at 2.2 AU (Dryer *et al.*, 1976; Intriligator, 1976; Ivanov, 1982). For example, a section in Ivanov (1982) focused on "shock waves from a series of flares", where complex IP streams originating from compound shock waves and their interaction region were described. Burlaga, Behannon, and Klein (1987) described a variety of compound streams resulting from the interaction of a transient with another transient or with a solar wind stream. They discussed the interaction of two ejecta, one con-

[1] http://www.helcats-fp7.eu.

taining a magnetic cloud and one without, as well as three shock waves and noted that "the compression of the magnetic cloud by shock S3 produced a magnetic field strength up to 36 nT".

The August 1972 series of eruptions resulted in a series of intense geomagnetic storms with the disturbed storm time (Dst) index peaking at −154 nT. Tsurutani *et al.* (1988) investigated the interplanetary origin of intense geomagnetic storms in the solar maximum of Solar Cycle 21, including cases related to the passage at Earth of a compound stream composed of multiple high-speed streams. Burlaga, Behannon, and Klein (1987) studied the 3 – 4 April 1979 event related to the interaction of two ejecta associated with an intense geomagnetic storm (Dst reached −202 nT) and discussed the relation between compound streams and large geomagnetic storms, finding that 9 out of 17 large geomagnetic storms for which interplanetary data were available were associated with compound streams (this includes CIR – CME as well as CME – CME interaction). To explain this result, they noted that "magnetic fields in ejecta can be amplified by the interaction with a shock and/or a fast flow and thereby cause a large geomagnetic storm" and concluded that "the interaction between two fast flows is in general a nonlinear process, and hence a compound stream is more than a linear superposition of its parts." Another multi-spacecraft study of compound streams measured in the late 1970s was performed by Burlaga, Hewish, and Behannon (1991).

Once again, the 2 – 7 August 1972 events revealed how series of flares and eruptions can result in an extremely high level of SEPs (Lin and Hudson, 1976). Sanderson *et al.* (1992) discussed *Ulysses* measurements of a shock propagating inside a shock-driving magnetic cloud and the low level of energetic particles between the two shocks. This was explained as the magnetic cloud "acting as a barrier delaying the onset of the high-energy protons from the second flare". Kallenrode *et al.* (1993) discussed super events associated with series of flares and CMEs.

Vandas *et al.* (1997) studied the interaction of a shock wave with a magnetic cloud using a 2.5 D magnetohydrodynamical (MHD) simulation. This study illustrates the power of numerical simulations, as a case with an overtaking shock was compared with an identical case without an overtaking shock. The authors noted that the shock propagation results in a radial compression of the magnetic cloud, a change of its aspect ratio, acceleration, and heating of the cloud.

In the remaining article, our focus is primarily on developments concerning the causes and consequences of series of CMEs that occurred since 2000. The combination of LASCO imaging and *in situ* measurements at L1 from *Wind* and/or ACE since 1996 makes it possible to relate coronal observations with their *in situ* consequences and geomagnetic effects. The study of CME – CME interaction proliferated following the report of two CMEs interacting within the LASCO-C3 field of view and associated type II event (Gopalswamy *et al.*, 2001) as well as the possible association of interacting CMEs with large SEP events (Gopalswamy *et al.*, 2002). Statistical surveys of geomagnetic storms and their interplanetary causes have become more routine during Solar Cycles 23 and 24 due to the reliability of L1 measurements; this has revealed how interacting CMEs may cause intense geomagnetic storms. In Solar Cycle 24, high spatial and temporal resolution observations by the *Solar Dynamics Observatory* (SDO: Pesnell, Thompson, and Chamberlin, 2012) have returned the study of sympathetic eruptions to central stage. The development of heliospheric imaging with the *Solar Mass Ejection Imager* (SMEI: Eyles *et al.*, 2003; Jackson *et al.*, 2004) and the HIs onboard STEREO have led to a large increase in the number of published cases of CME – CME interaction being remotely observed. Last, the development of large-scale time-dependent numerical simulations in the past 20 years have yielded new insights into the mechanisms resulting in the initiation of series of CMEs, as

well as the physical processes occurring during their propagation and interaction. This article is organized as follows. In Section 2 we discuss recent developments regarding the initiation of successive CMEs, including observations and numerical simulations of sympathetic and homologous CME initiation. In Section 3 we review observational and theoretical works focusing on the association of successive and interacting CMEs with large SEP events and with enhanced and unusual radio emissions. In Section 4 we focus on the physical processes occurring during CME – CME interaction in the inner heliosphere, with insights gained from recent remote observations by SECCHI as well as by numerical simulations and the analysis of *in situ* measurements. In Section 5 we discuss how the complex ejecta resulting from CME – CME interaction may drive Earth's magnetosphere in unusual ways, often producing large geomagnetic storms, but also sometimes weaker-than-expected storms. In Section 6 we discuss what to expect in the upcoming decade with new observations closer to the Sun made possible by *Solar Probe+* and *Solar Orbiter* and conclude.

2. Initiation of Successive CMEs

2.1. Trigger and Initiation of CMEs

As the largest explosive phenomenon on the Sun, a typical CME carries about 10^{32} erg of energy (Vourlidas *et al.*, 2000; Hudson, Bougeret, and Burkepile, 2006) and 10^{21} Mx of magnetic flux (Dasso *et al.*, 2005; Qiu *et al.*, 2007; Wang *et al.*, 2015) into IP space, which is associated with a reconfiguration of coronal magnetic fields in the CME source region. To support such large eruptions, the following is required: (1) sufficient magnetic free energy, and (2) triggers and efficient energy conversion processes to release the free energy on a short timescale. The magnetic free energy as well as helicity can be accumulated gradually in various ways, *e.g.* flux emergence (see, *e.g.*, Heyvaerts, Priest, and Rust, 1977; Chen and Shibata, 2000), or shearing/rotational motion (see, *e.g.*, Manchester, 2003; Brown *et al.*, 2003; Kusano *et al.*, 2004; Zhang, Liu, and Zhang, 2008). It is often found that the magnetic free energy accumulated in an active region (AR) exceeds the energy required for an eruption. A well-studied case is AR 11158, which has been examined based on the SDO/HMI vector magnetograms (see, *e.g.*, Schrijver *et al.*, 2011; Sun *et al.*, 2012; Wang *et al.*, 2012; Vemareddy, Ambastha, and Maurya, 2012). With the aid of a nonlinear force-free field (NLFFF) extrapolation method (Wiegelmann *et al.*, 2012), Sun *et al.* (2012) investigated the evolution of the magnetic field and its energy in the AR from 12 – 17 February 2011. It was found that the magnetic energy continuously increased, with the free energy well above 10^{32} erg. The only X-class flare during the period of interest consumed only a small fraction of the accumulated free energy (on the order of 10 – 20%). Thus, a pivotal and highly unclear issue is what the effective triggers of the free energy release are.

It is now acknowledged that there are generally two types of triggering mechanisms. The first is a non-ideal process, associated with magnetic reconnection. The tether-cutting model (Moore *et al.*, 2001) and magnetic breakout model (Antiochos, DeVore, and Klimchuk, 1999) are both of this type. The other is loss of equilibrium, an ideal process, due to some instabilities, *e.g.* the kink instability (see, *e.g.*, Hood and Priest, 1979, 1980), torus instability (see, *e.g.*, Török, Kliem, and Titov, 2004; Kliem and Török, 2006; Fan and Gibson, 2007), and catastrophe (Forbes and Priest, 1995; Lin and Forbes, 2000; Hu, 2001).

CMEs are large-scale structures that may involve multiple magnetic flux systems, but trigger points usually start locally. The question whether the CME occurrence is random naturally arises. In other words, can one CME trigger another CME, and if yes, how? A way

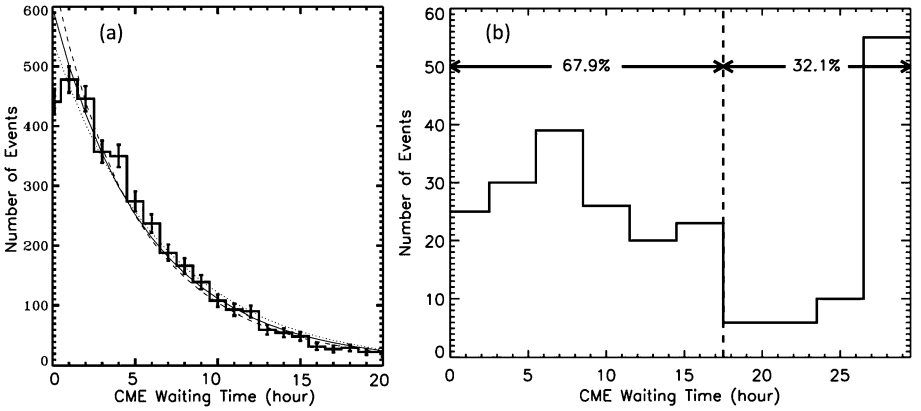

Figure 1 (a) Adapted from Moon *et al.* (2003b), showing the waiting time distribution of all CMEs during October 1998 – December 2001. For comparison, a stationary Poisson distribution (dotted line) and two non-stationary Poisson distributions (dashed and solid lines) are plotted. (b) Adapted from Wang *et al.* (2013), showing the waiting time distribution of quasi-homologous CMEs originating from all the CME-rich super ARs in Solar Cycle 23. The two panels are reproduced by permission of the American Astronomical Society (AAS).

to test the degree of interdependence of CMEs is through a statistical approach. An early attempt to examine the independence of CMEs was made by Moon *et al.* (2003b), who considered 3817 CMEs listed in the LASCO CME catalog (Yashiro *et al.*, 2004) during 1999 – 2001. They generated the waiting time distribution of these CMEs in terms of their first appearance in the field of view of LASCO-C2 and found that it is very close to an exponential distribution (Figure 1a) and can be well explained by a time-dependent Poisson random process. A similar distribution can also be found in solar flares (Wheatland, 2000). These results imply that interrelated CMEs only constitute at most a small fraction of the whole population of CMEs.

On the other hand, modern observations have shown numerous pieces of evidence that some CMEs do not occur independently from each other. Such interrelations can be also found in other explosive phenomena, such as flares and filament eruptions, which are generally referred to as "sympathetic" eruptions (see, *e.g.*, Richardson, 1951; Fritzova-Svestkova, Chase, and Svestka, 1976; Pearce and Harrison, 1990; Biesecker and Thompson, 2000; Wang *et al.*, 2001, 2016; Moon *et al.*, 2002; Schrijver and Title, 2011; Jiang *et al.*, 2011; Shen, Liu, and Su, 2012; Yang *et al.*, 2012). In general, sympathetic CMEs refer to those originating from different regions, but almost simultaneously (Moon *et al.*, 2003b), whereas the eruptions occurring successively from the same region in a relatively short interval (several hours) that have a similar morphology and similar associated phenomena are referred to as homologous CMEs (Zhang and Wang, 2002) or are generally called "quasi-homologous" CMEs regardless of their morphology and associations (see, *e.g.*, Chen *et al.*, 2011; Wang *et al.*, 2013). The two types of interrelated CMEs are potential candidates for CME – CME interactions, and such interactions may begin during the initiation and last all the way to the IP space. Thus, it becomes of particular interest to determine under which circumstances CMEs are triggered successively.

2.2. Homologous CMEs

The possibility that the Sun produces homologous eruptions based on their similar visual aspects and origins was raised at the beginning of space-based coronal observations using

ground-based coronagraphs, as well as the coronagraph onboard the *Orbiting Solar Observatory 7* (OSO-7: Hansen *et al.*, 1974). Although the waiting times of all CMEs are approximately exponentially distributed, a quite different distribution can be found when only the waiting times for CMEs originating from the same ARs are considered. Based on the source locations of all the CMEs during 1997 – 1998 (Wang *et al.*, 2011), Chen *et al.* (2011) investigated 15 CME-rich ARs that produced more than 80 quasi-homologous CMEs, and analyzed the waiting times between CMEs from the same AR. It was found that the distribution has two components, clearly separated at around 15 hours. The component within 15 hours follows a Gaussian-like distribution with the peak at around 8 hours, and it is thought to represent physically related events. The CMEs in the other component are most likely to be independent. Wang *et al.* (2013) extended the sample to all the CME-rich super ARs in Solar Cycle 23, covering 281 CMEs, and found a similar distribution of the waiting times of the CMEs (Figure 1b). The only difference is that the separation time of the two components slightly increases from 15 hours to 18 hours and the peak of the Gaussian-like component decreases to around 7 hours. In this way, we may refine the definition of quasi-homologous CMEs as the successive CMEs originating from the same AR with a separation smaller than $\sim 15 - 18$ hours.

This finding raises two subsequent questions: how are the quasi-homologous CMEs physically related, and what causes the second CME? The Gaussian-like component of the waiting time distribution suggests that either (1) the magnetic free energy and/or helicity accumulate and reach a threshold on a pace of about 7 hours on average, or (2) the timescale of the growth of the instability of a loop system triggered by the preceding CME is about 7 hours. The former mechanism is applicable to the quasi-homologous CMEs originating from the same polarity inversion lines (PILs), whereas the latter is for those from the different parts of a PIL or neighboring PILs even though they are in the same AR. This picture is worthy of further validations with observations.

One widely studied case is the homologous CMEs occurring from AR 9236 on 24 – 25 November 2000 (see, *e.g.*, Nitta and Hudson, 2001; Zhang and Wang, 2002; Moon *et al.*, 2003a). In a 60-hour interval, a total of six halo CMEs associated with five X-class and one M-class flares originated from the AR. By combining *Yohkoh* X-ray data and SOHO/MDI magnetograms, Nitta and Hudson (2001) showed that all of the associated flares occurred around the leading spot of the AR. The first four flares successively originated from the western part of the spot with the emission intensity decreasing. The intensity of the last two flares increased, but originated from the southern part of the spot. The hard X-ray footpoints were located in different regions for the first four flares as compared to the last two flares, suggesting that the two sets of CMEs might originate from the different PILs. Since many small polarity pairs emerged into the spot during the period, Nitta and Hudson (2001) suggested that the continuously emerging magnetic flux was the cause of the successive CMEs and flares. In more detail, Zhang and Wang (2002) investigated the magnetic flux emergence around the flaring regions for the first three eruptions. They used time-sequences of the high-resolution MDI magnetograms to follow the evolution of 452 moving magnetic features from their births to deaths, and found that there were three flux peaks in the temporal evolution that corresponded well to the occurrence of the eruptions. The calculation of the magnetic helicity based on the MDI magnetograms also showed that there were significant spikes in the helicity change rate during the eruptions (Moon *et al.*, 2003a). These results match the first aforementioned scenario that the rebuilding of free energy is probably a key mechanism for the homologous CMEs. It is noteworthy that the first three CMEs in the series traveled with increasing speeds from about 700 to 1000 $\mathrm{km\,s^{-1}}$ and were followed by another extremely fast CME with a speed of > 2000 $\mathrm{km\,s^{-1}}$ originating from a different

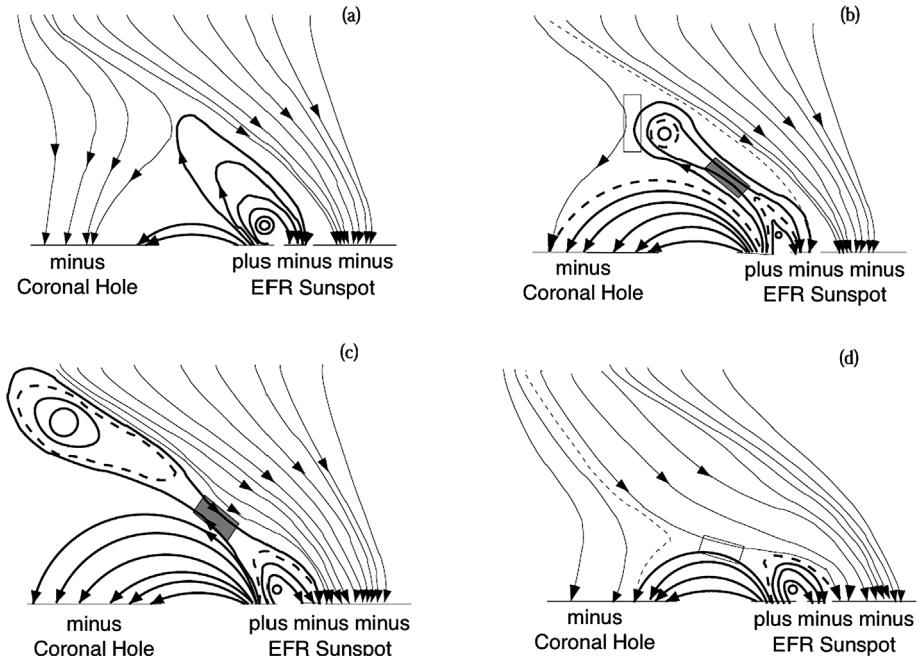

Figure 2 Schematic diagram illustrating the process of continuously emerging fluxes causing homologous CMEs (directly adapted from Sterling and Moore, 2001). The rectangles indicate the reconnection regions. Reproduced by permission of the AAS.

region (Nitta and Hudson, 2001). These four successive CMEs interacted in interplanetary space and formed a complex structure at 1 AU (Wang, Wang, and Ye, 2002, also see Section 4.4).

The process of how the continuously emerging fluxes cause homologous CMEs was previously proposed by Sterling and Moore (2001) based on the breakout picture (Antiochos, DeVore, and Klimchuk, 1999). They studied two homologous CME-associated flares from AR 8210 on 1 – 2 May 1998 and found signatures of reconnection between the closed field of the emerging flux and the open field in a neighboring coronal hole. This led to a series of CMEs, as the whole process repeats (see Figure 2). Nevertheless, two homologous CMEs reported and studied by Chandra *et al.* (2011) seemed to have different triggering mechanisms. The two CMEs originated from AR 10501 on 20 November 2003, associated with homologous Hα ribbons. By applying a linear force-free field (LFFF) extrapolation method (Démoulin *et al.*, 1997), the authors identified the quasi-separatrix layers in 3D, and compared with the locations of flaring ribbons. They suggested that the first CME and flare were triggered by the tether-cutting process, which manifested itself as a significant shear motion and reconnection below the core field, and resulted in a destabilized magnetic configuration for the second CME and flare, which were more likely to be initially driven by an instability or a catastrophic process. A similar case was reported by Cheng *et al.* (2013), who studied two successive CMEs originating on 23 January 2012, and found that the first CME partially removed the overlying field and triggered the torus instability for the second CME one and half hours later. These two eruptions have also been studied in detail by Li and Zhang (2013), Joshi *et al.* (2013), and Sterling *et al.* (2014), and their interplanetary consequences by Liu *et al.* (2013). Another example was the two eruptions separated by about

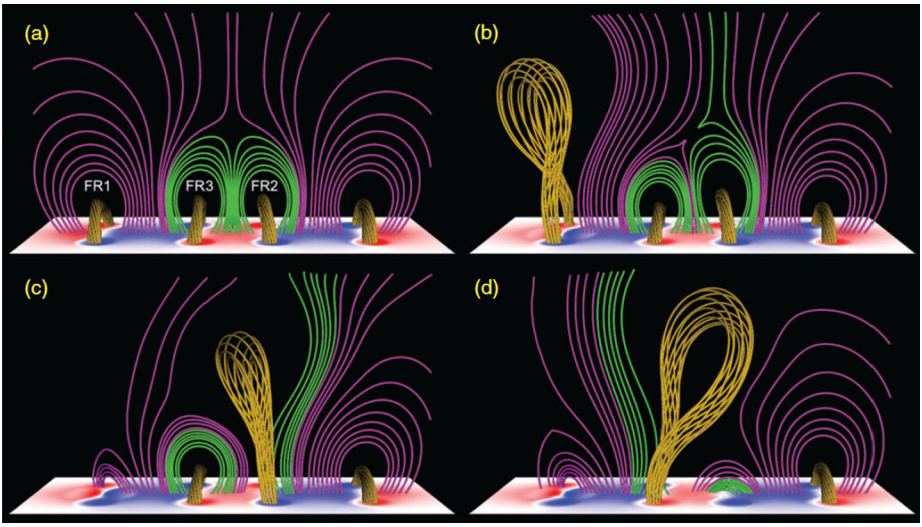

Figure 3 Numerical simulations showing the trigger and initiation of successive CMEs (adapted from Török *et al.*, 2011). The flux ropes, original closed field lines, and open field lines are indicated in yellow, green, and purple, respectively. Reproduced by permission of the AAS.

50 minutes on 7 March 2012 from AR 11429 analyzed by Wang *et al.* (2014a), who studied the magnetic field restructuring and helicity injection changes before and during these two successive eruptions.

Regarding to the time delay between (quasi-)homologous CMEs, an extreme case is that two CMEs originate from one AR at almost the same time, *i.e.* within minutes, the so-called "twin-CME" scenario (Li *et al.*, 2012). One such case was reported by Shen *et al.* (2013a), two CMEs launched from AR 11476 within about 2 minutes, based on high-resolution and high-cadence observations from SDO. SDO/HMI magnetograms suggest that the CMEs originated from two segments of a bent PIL, above which a mature flux rope and a set of sheared arcades were located, as revealed by an NLFFF extrapolation. The twin-CMEs caused the first ground-level enhancement (GLE) event in Solar Cycle 24 on 17 May 2012, consistent with the statistical studies that interaction of two CMEs launched in close temporal succession favors particle accelerations (see, *e.g.*, Li *et al.*, 2012; Ding *et al.*, 2013). More discussions about the effect of interacting CMEs on particle accelerations are continued in Section 3.

Such successive CMEs from the same AR can be studied in numerical simulations either by supplying free energy into the system through flux emergence (MacTaggart and Hood, 2009; Chatterjee and Fan, 2013), through continuous shear motions (DeVore and Antiochos, 2008; Soenen *et al.*, 2009), or by the perturbation of previously neighboring eruptions (Török *et al.*, 2011; Bemporad *et al.*, 2012). The latter may be treated as a kind of CME – CME interaction during the initiation phase. The simulation by Török *et al.* (2011) was established on a set of zero-β compressible ideal MHD equations (Török and Kliem, 2003) in which four flux ropes (Titov and Démoulin, 1999) were inserted, with two of them under a pseudo-streamer and the other two placed on each side of the pseudo-streamer. After the triggering of the eruption of one flux rope next to the pseudo-streamer, the whole simulated system becomes unstable (see Figure 3). The first erupted flux rope expands as it rises and causes breakout reconnection above one of the flux ropes beneath the pseudo-streamer,

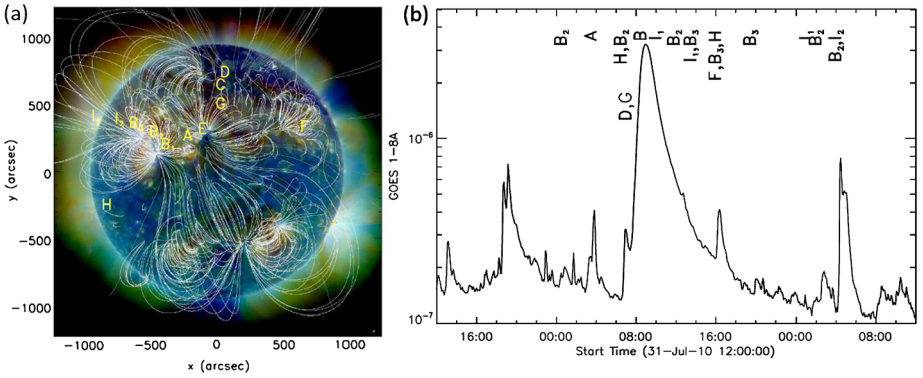

Figure 4 (a) Three-color composite EUV image combined from SDO/AIA 211Å, 193Å, and 171Å channels on 1 August 2010. Coronal magnetic field lines extrapolated using a potential field source surface (PFSS) model are superimposed, showing the magnetic connections among different regions. Letters denote the locations of the eruptive events during 1 – 2 August 2010. (b) GOES 1 – 8 Å light curve with the same denoted letters. Adapted from Schrijver and Title (2011).

which leads to the second eruption. As a consequence, a vertical current sheet forms beneath the second erupted flux rope and reconnection occurs, which results in a third eruption. Both the second and third eruptions are due to the weakening of the constraints of the overlying fields, suggesting that the torus instability plays a pivotal role in the successive eruptions. The second and third eruptions come from the same pseudo-streamer and therefore match the picture of quasi-homologous CMEs from the same AR, but different PILs. The typical timescale of the torus instability, which leads to the third eruption, is of interest, as the statistical analysis suggests about 7 hours. However, studies on this point are rare. In addition, the above simulation results might be also applicable to sympathetic CMEs, which are discussed next.

2.3. Sympathetic CMEs

As defined earlier, sympathetic CMEs originate almost simultaneously, but from spatially separated regions, and one eruption contributes to the triggering of another. Lyons and Simnett (1999) mentioned the possibility for "one CME [to] activate the onset of another", whereas Moon *et al.* (2003b) are the first to specifically use the term "sympathetic CMEs". Defining the term "simultaneously" quantitatively is a complex problem. In most studies, it refers to a temporal separation between the eruptions of less than several hours. Thus, in this aspect, sympathetic CMEs are similar to those quasi-homologous CMEs originating from different PILs in the same AR. The key question for sympathetic CMEs is how distant magnetic systems connect and interact with each other in such a short interval. The study by Simnett and Hudson (1997) showed that the CME occurring on 23 February 1997 erupted from the northeast limb of the Sun and quickly merged with a previously much larger event, which was associated with a loop system connecting the northern region to the southern region (another example can be found in Figure 4). Such transequatorial loops are common. A statistical study based on *Yohkoh* data from October 1991 to December 1998 showed that one third of all ARs present transequatorial loops (Pevtsov, 2000), suggesting that ARs can be magnetically connected even though they are located on the opposite hemispheres of the Sun (see also Webb *et al.*, 1997).

Wang *et al.* (2001) presented a case of the connection between two M-class sympathetic flares from two different ARs (referred to as inter-AR interaction). The two flares were separated by about 1.5 hours and originated from ARs 8869 and 8872 on 17 February 2000. Both were associated with a filament. During the progress of the first flare, the associated filament disappeared and a loop structure connecting the two flaring regions became visible in Hα images. Along the path of the loop, a surge starting from one end of the erupted filament quickly excited a set of disturbances propagating toward the other AR, which was followed by the second flare and the second filament disappearance. The speed of the disturbances was estimated as about 80 $\mathrm{km\,s^{-1}}$, close to the local Alfvén speed. Another similar interaction between two eruptions was presented in Jiang *et al.* (2008), in which a transequatorial jet disturbed inter-AR loops and led to their eruption. The jet and the loop eruptions drove two CMEs separated by less than 2 hours. Combining multiwavelength observations including the higher-resolution data from SDO, Joshi *et al.* (2016) recently described sympathetic eruptions in two adjacent ARs on 17 November 2013. A scenario of a series of chain reconnections was proposed for these eruptions with the aid of an NLFFF extrapolation.

Such connections or interactions are not limited to adjacent ARs. Thanks to the stereoscopic observations provided by the STEREO twin spacecraft, as well as SOHO and SDO near the Earth, the global connections among flares and CMEs originating from different regions can be explored. A well-studied series of events are the interrelated eruptive events during 1 – 2 August 2010 (see, *e.g.*, Schrijver and Title, 2011; Harrison *et al.*, 2012; Liu *et al.*, 2012). The study by Schrijver and Title (2011) focused on the near-synchronous long-distance interactions between magnetic domains. They identified more than ten events, including flares, filament eruptions, and CMEs. With the aid of a magnetic field extrapolation method based on the potential field assumption, they investigated the global topology of the magnetic field and its changes. It was found that all the scattered major events were connected via large-scale separators, separatrices, and quasi-separatrix layers. These results are consistent with the study by Titov *et al.* (2012), who also reconstructed the topology of the coronal magnetic field and investigated the connections between the eruptions and the pseudo-streamers, separatrices, and quasi-separatrix layers. They proposed that reconnections along these separators triggered by the first eruption probably caused the sequential eruptions. The resulting CMEs interacted with each other during their propagation in interplanetary space. A more complete picture of this series of events is given in Harrison *et al.* (2012) and Liu *et al.* (2012). The long-distance coupling was further studied with more events by Schrijver *et al.* (2013). They argued that there are several distinct pathways for sympathetic eruptions, *e.g.* waves or propagating perturbations, distortion of or reconnection with the overlying field by distant eruptions, and other (in)direct magnetic connections.

The simulations by Török *et al.* (2011), mentioned in Section 2.2, reproduced the successive CMEs from the regions beneath and beside a pseudo-streamer (Figure 3), which is not only applicable to the eruption of quasi-homologous CMEs from one AR, but also to the possible long-distance coupling between different ARs. In their simulations, the breakout reconnection and weakening of overlying fields due to the neighboring eruptions are responsible for sequential eruptions. The same process was reproduced in the 2.5D MHD simulations by Lynch and Edmondson (2013). With a full 3D MHD code under the Space Weather Modeling Framework (Tóth *et al.*, 2005, 2012; van der Holst *et al.*, 2014), Jin *et al.* (2016) numerically studied the long-distance magnetic impacts of CMEs. The coronal environment on 15 February 2011 was established and a CME was initiated by inserting a flux rope of the Gibson and Low (1998) analytical solution into AR 11158. The impacts of the CME on eight ARs, five filament channels, and two quiet-Sun regions were evaluated by the

decay index, defined as $-\frac{d\log B(h)}{d\log h}$, where B is the magnetic field and h is the height above the solar surface, and other impact factors. They found that the impact weakens at longer distances and/or for stronger magnetic structures, and suggested that there were two different types of the impacts. The first is the direct impact due to the CME expansion and the induced reconnection, which may efficiently weaken the overlying field. It is limited spatially to the CME expansion domain. The second is the indirect impact outside the CME expansion domain, where the impact of the CME is propagated through waves during both the eruption and the post-eruption phases, and the overlying field may be weakened, especially when the global magnetic field relaxes to a steady state during the post-eruption phase.

Although the mechanisms of long-distance coupling have been extensively studied and well documented, it is still unclear under which circumstances a CME may successfully take off. That is to say, not all of the regions impacted by a CME do launch a sequential CME. The same issue holds for (quasi-)homologous eruptions.

3. Effects of Successive CMEs on Particle Acceleration

3.1. Successive CMEs and Solar Energetic Particle Events

Solar energetic particles (SEPs) are known to be accelerated in association with two main phenomena: solar flares and CMEs. Historically, SEPs have been divided into impulsive events of shorter duration, most often associated with solar flares, but not always (Kahler, Reames, and Sheeley, 2001), and gradual events, most often associated with CME-driven shocks (Cane, McGuire, and von Rosenvinge, 1986; Reames, 1999; Cliver, Kahler, and Reames, 2004). There are typically significant differences between SEPs accelerated through these two mechanisms, including the duration, elemental abundances, spectra, *etc.* (Mason, Mazur, and Dwyer, 1999; Desai *et al.*, 2003, 2006; Tylka *et al.*, 2005). In the past two decades, with remote observations of CMEs and *in situ* measurements of SEPs, it has become well established that the largest gradual SEP events are associated with fast and wide CMEs (Kahler, 1992; Reames, 1990; Zank, Rice, and Wu, 2000). Large CME shock fronts are ideal accelerators for charged particles, and therefore SEPs can occasionally reach energies of up to several GeVs. SEPs together with cosmic rays play an important role in space weather (see, *e.g.*, Usoskin, 2013).

The magnetic field configuration is crucial in order to determine whether accelerated particles might be detected. For Earth-affecting SEP events, the particles are thought to be injected into field lines located in the western hemisphere of the Sun, accounting for Sun – Earth connecting magnetic structures due to the Parker spiral shape of the IP magnetic field (see, *e.g.*, Klein *et al.*, 2008; Schwenn, 2006). Therefore, fast CMEs originating from the western hemisphere of the Sun are more likely to be magnetically connected to Earth; and hence, fast and wide western-limb CMEs are the most common cause of large gradual SEP events (Cane, Reames, and von Rosenvinge, 1988; Gopalswamy, 2004). There are also large SEP events observed with clear sources from the eastern solar hemisphere. From STEREO observations, with widely separated spacecraft, it is recognized that SEPs are indeed a widespread phenomena (see, *e.g.*, Dresing *et al.*, 2012). However, a simple look at SEP and CME statistics reveals that not all fast, wide, and western CMEs are associated with large SEP events (Ding *et al.*, 2013).

Different scenarios of acceleration processes for electrons and ions have been discussed (see, *e.g.*, Kliem *et al.*, 2003). Among others, coronal waves, CME lateral expansion, and CME – CME interaction are possible candidates. Studies on Moreton and EUV waves are

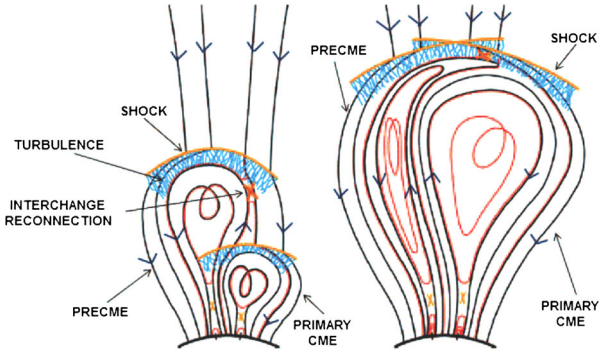

Figure 5 Twin-CME scenario first outlined by Li *et al.* (2012) and adapted by Kahler and Vourlidas (2014). Left: the preCME drives a turbulent shock region (blue shaded area). The SEP-producing CME (primary CME) is launched close to the preCME, but later in time. The magnetically accessible (interchange reconnection, marked by orange crosses) turbulent shock region in the preCME acts as amplifier for particles accelerated by the shock of the primary CME. Right: the more developed phase of the preCME – CME interaction, where the primary CME shock has crossed the reconnection region.

still unresolved and cannot fully rule out coronal waves as the SEP driving agent (against: Bothmer *et al.*, 1997; Krucker *et al.*, 1999; Miteva *et al.*, 2014; pro: Malandraki *et al.*, 2009; Rouillard *et al.*, 2012). CME – CME interaction itself might play a minor role in the SEP production, but a preceding CME might have a significant effect in terms of preconditioning. This idea originated from a statistical study by Gopalswamy *et al.* (2002), which showed that the presence of a previous CME within 12 hours of a wide and fast CME greatly increases the probability that this second fast CME is SEP-rich (Gopalswamy *et al.*, 2002; Gopalswamy, 2004). The reverse relation was also found: SEP-rich CMEs are about three times more likely than average to be preceded by another eruption (Kahler and Vourlidas, 2005). In another study of 57 large SEP events that had intensities > 10 pfu (particle flux units, 1 pfu $= 1$ proton $\mathrm{cm}^{-2}\,\mathrm{s}^{-1}\,\mathrm{sr}^{-1}$) at > 10 MeV/nuc, Gopalswamy (2004) showed that a strong correlation exists between high particle intensities and the presence of preceding CMEs within 24 hours of the main SEP-accelerating CME. As the acceleration of SEPs is believed to occur within the first 10 $R_{\odot}$ (and most likely within the first 4 – 5 $R_{\odot}$), this time line makes it less probable that direct shock – shock interaction is responsible for the observed higher probability of SEP events (Richardson *et al.*, 2003; Kahler, 2003). While important, these studies are not enough to determine the physical causes of these statistical relations. Hence, the role of interacting CMEs and their relation to large SEP events still leaves many questions open.

The preconditioning of the ambient environment close to the Sun has important effects on SEP production. 1) Preceding CMEs (pre-CMEs) not only can provide an enhanced seed population, but also lead to a stronger turbulence at the second shock, thereby increasing the maximum energy of the particles (this is referred to as the twin-CME scenario, as proposed by Li and Zank (2005) and further developed in Li *et al.* (2012); see Figure 5 and Section 2.2). Ding *et al.* (2013, 2014a) tested the twin-CME scenario against all large SEP events and fast CMEs with speeds > 900 km s^{-1} from the western hemisphere in Solar Cycle 23. They suggested that a reasonable choice of the time threshold for separating a single CME and a twin-CME is 13 hours. Using this time delay, they found that 60% of the twin-CMEs lead to large SEPs, while only 21% single CMEs lead to large SEPs. Furthermore, all large SEP events with a peak intensity higher than 100 pfu at > 10 MeV/nuc recorded by the *Geostationary Operational Environmental Satellite* (GOES)

are twin-CMEs. Note that twin-CMEs may or may not be associated with direct interaction between the CMEs themselves. 2) The change in nature of closed and open magnetic field lines in the vicinity of an AR may result in a different shock angle. Tylka *et al.* (2005) and Sokolov *et al.* (2006), among others, have shown that the shock geometry can have a large influence on the SEP flux and intensity. 3) The presence of closed field lines within a CME might trap particles that are accelerated by a subsequent CME, and hence decrease the flux of high-energy particles at Earth (Kahler, 2003) or increase their maximum energy (Gopalswamy, 2004). 4) On longer timescales, the presence of a CME in the heliosphere might dramatically modify the Sun – Earth magnetic connectivity, the length and solar footprints of the field lines connected to Earth. This is clearly visible when an SEP event occurs while an interplanetary CME (ICME) passes over Earth (Kallenrode, 2001; Ruffolo *et al.*, 2006). This type of configuration usually results in delaying SEPs, but it might also significantly change the Sun – Earth connectivity (Richardson, Cane, and von Rosenvinge, 1991). Masson, Antiochos, and DeVore (2013) investigated how flare-accelerated SEPs may reach open field lines through magnetic reconnection during a CME-associated flare. Similar processes need to occur during CME – CME interaction for accelerated particles to be measured at Earth.

Although the association of preceding CMEs with enhanced SEP intensity is a robust observation, alternative explanations to the twin-CME scenario exist. In a recent work, Kahler and Vourlidas (2014), making use of an extensive SEP list from Kahler and Vourlidas (2013), found a relation between the 2 MeV proton background intensities and an increase in the SEP event intensities and the occurrence rates of preceding CMEs. They suggested that preceding CMEs may be an observational signature of enhanced SEP intensities but are not physically coupled with them. This is in contradiction to the events studied in Gopalswamy (2004) and Ding *et al.* (2013), for which no association of larger SEP events with >2 MeV backgrounds is found. We note that most of the CME-related studies are based on the LASCO CME catalog (Yashiro *et al.*, 2004), which contains measurements of CME kinematics and hence energies at heights too far away (beyond 10 $R_{\odot}$) to be directly compared with particle energies. Therefore the importance of the background effect remains unclear, as well as whether 2 MeV particles are the right energy level to study "seed" particles for SEPs.

3.2. Radio Signatures of CME – CME Interaction

Closely related to CMEs and SEP production processes, and most probably more closely related to CME – CME interaction events, is the observation of enhanced radio emission for CME – CME events. Gopalswamy *et al.* (2001) first reported radio signatures in the long-wavelength range that occurred as intense continuum-like radio emission following an interplanetary type II burst. They linked the timing of the enhancement in the radio emission to the overtaking of a slow CME by a faster one. As shown in Figure 6, enhanced radio signatures as consequence of CME – CME interaction are in fact frequently reported (see, *e.g.*, Reiner *et al.*, 2003; Hillaris *et al.*, 2011; Martínez Oliveros *et al.*, 2012; Ding *et al.*, 2014b; Temmer *et al.*, 2014). We note that the description of such a scenario is intimately connected to the 3D geometry and propagation direction of two CMEs. While many of the studies are in agreement that the CME interaction is the cause of the radio enhancement, the interpretation is not straightforward. We review this process step by step.

Type II radio bursts give information on the propagation and density behavior of the CME-associated shock component (Mann, Classen, and Aurass, 1995). As a consequence of interacting CMEs, a continuum-like enhancement of decametric to hectometric (dm

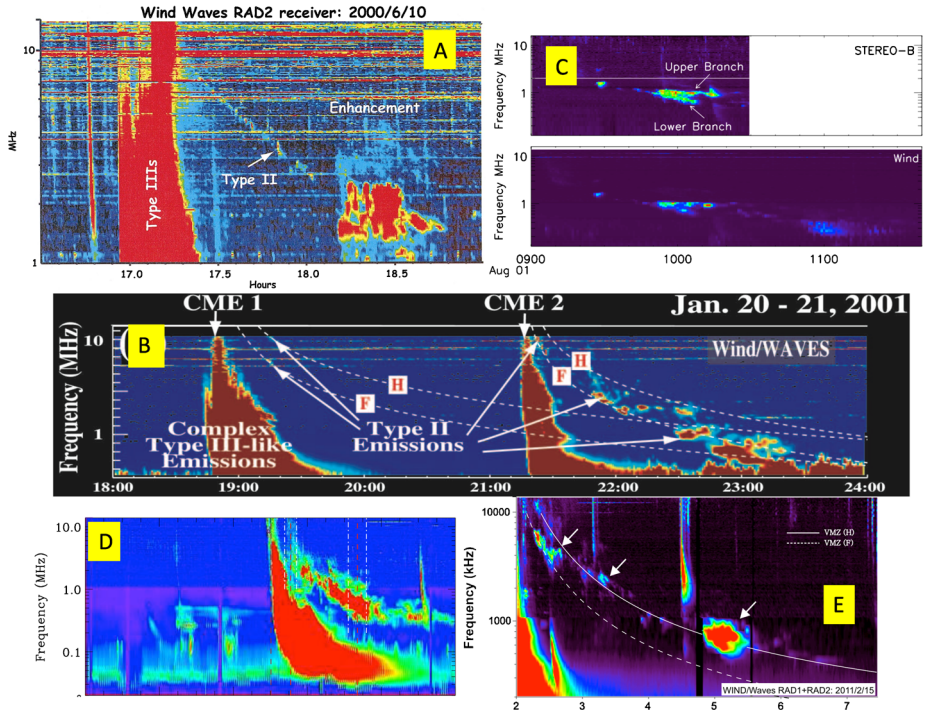

Figure 6 Selection of observations for enhanced type II radio bursts associated with CME – CME interaction events (identified by the solar event naming convention – solar object locator SOL): a) Gopalswamy *et al.* (2001) (SOL-2000-06-10); b) Reiner *et al.* (2003) (SOL-2001-01-20); c) Martínez Oliveros *et al.* (2012) (SOL-2011-08-01); d) Ding *et al.* (2014b) (SOL-2013-05-22); e) Temmer *et al.* (2014) (SOL-2011-02-15).

to hm) type II radio emission may be interpreted as observational signature of the transit of the shock front of the fast CME through the core of the slow CME. This presumes that the upstream compression due to the passage of a CME enhances the particle density and therefore decreases the background Alfvén velocity, which would result in a stronger shock (Gopalswamy, 2004; Kahler and Vourlidas, 2005; Li and Zank, 2005). However, the collision not only increases the electron density due to compression, but also the magnetic field. In fact, the Alfvén speed is expected to be higher inside a CME that would actually lead to a reduction of the shock Mach number (Kahler, 2003; Klein, 2006). Even with higher coronal density, this would make the overtaking shock weaker and less likely to occur. Numerical simulations show that in CME – CME interaction events, large variations in density, Alfvén speed, and magnetic field can be expected within the preceding CME (Lugaz, Manchester, and Gombosi, 2005). In this respect, we note that a reduced Alfvén speed within the structures would reduce the efficiency of reconnection processes and CME "cannibalism" might not work efficiently. This is confirmed by *in situ* measurements from CME – CME interaction events showing rather intact separate flux ropes for the CME – CME interaction events (see, *e.g.*, Martínez Oliveros *et al.*, 2012). Nevertheless, the merging process is taking place as shown, among others, by Maričić *et al.* (2014), where possible reconnection outbursts from *in situ* data at 1 AU are observed for the CME – CME interaction event series from 13 – 15 February 2011. However, the time span needed to merge two flux ropes completely might be too short and might only be observed

beyond distances of 1 AU – more details about CME – CME interaction processes are found in Section 4.

Ding *et al.* (2014b) and Temmer *et al.* (2014) are two of the few examples using stereoscopic observations with the Graduated Cylindrical Shell (GCS) model of Thernisien (2011) to determine the real direction and heights of two successively erupting CMEs rather than plane-of-sky heights and projected directions. Using this approach, Ding *et al.* (2014b) found that the start time of type II radio emissions coincided with the interaction between the front of the second CME and the trailing edge of the first CME, interaction which occurred around 6 $R_{\odot}$, also close to the distance of peak SEP acceleration. This is not supported by Temmer *et al.* (2014), who concluded that the timing for the enhanced type II bursts did not match the time of interaction for the CMEs, but they could be related to a kind of shock-streamer interaction (Shen *et al.*, 2013b). In the event under study, the flanks of the following CME might interact with the field, which was opened and compressed by the preceding CME. Another scenario describing the occurrence of continuum-like radio emissions might be reconnection processes of the poloidal field components between the interacting CMEs (Gopalswamy, 2004). In fact, enhanced type II radio signatures may be the signatures of several different types of interactions.

Information on the magnetic field topology involved in the process of CME – CME interaction might be given by radio type III bursts. Radio type III bursts are generated by energetic electron beams guided along quasi-open magnetic field lines. Owing to a sudden change in the magnetic topology, type N radio bursts in addition show a drift in the opposite direction (classical interpretation: magnetic mirror effect). As CMEs manifest themselves as sudden change in the generally outward directed IP magnetic field and electron density distribution, Démoulin *et al.* (2007) conclude that decametric type N radio bursts are most likely not caused by mirroring effects, but are due to geometry effects as a consequence of the magnetic restructuring in CME – CME interaction events. Hillaris *et al.* (2011) report on peculiar type III radio bursts that are due to accelerated electrons that might be disrupted by the turbulence near the front of a preceding CME (see also Reiner and Kaiser, 1999). Results from Temmer *et al.* (2014) showed that the observed type II enhancements, which were associated with type III bursts, stopped at frequencies related to the downstream region of the extrapolated type II burst, as if it were a barrier for particles entering the magnetic structure (MacDowall, 1989).

In this respect, there have been several attempts to explore the magnetic connectivity to interplanetary observers. Some of them have used realistic MHD simulations combined with a simple particle source input at the inner boundary in the inner heliosphere and ballistic particle propagation (Luhmann *et al.*, 2010), while others employ an idealized shock surface and Parker spiral, together with physics-based transport (Aran *et al.*, 2007; Rodríguez-Gasén *et al.*, 2014). Masson *et al.* (2012) investigated the interplanetary magnetic field configurations based on observations during ten GLE events and concluded that particle arrival times were significantly later than what would be expected under a Parker spiral field, illustrating how the magnetic connectivity to a given observer cannot be assumed to be static. It may be modified before and during the eruption by other structures between the Sun and the Earth, such as other CMEs, solar wind streams, and corotating interaction regions (CIRs), or by reconnection occurring close to the solar surface. Recently, Kahler, Arge, and Smith (2016) tested the appropriateness of the Parker's spiral approximation for SEP studies using the Wang–Sheeley–Arge (WSA: Wang and Sheeley, 1990; Arge and Pizzo, 2000) model, and reached similar conclusions. One limitation of these studies is that none of them includes a magnetic ejecta driving a shock wave that is initiated in the low corona, *i.e.* where particle acceleration is known to occur.

The significant drawback in these observational studies comes from the limitation of currently available data, which may only reveal the consequences of CME – CME interaction, but not the interaction process itself. A more direct insight into the CME – CME interaction process and related plasma and magnetic field parameters could be gained from *in situ* data. However, most of CME events collide far from where plasma and magnetic field parameters are actually monitored. An exception is the 30 September 2012 event, which revealed interaction between two CMEs close to 1AU (probably started interacting $\sim$0.8 AU), as shown in studies by Liu *et al.* (2014b) and Mishra, Srivastava, and Singh (2015). The *in situ* instruments onboard *Solar Orbiter* and *Solar Probe+* (to be launched in 2018), which will travel at close distances to the Sun, will be of great interest and will give a great complementary view on the CME – CME interaction processes.

4. The Interaction of CMEs in the Inner Heliosphere

Direct observations of CME – CME interaction became possible in the mid 1990s with the larger field of view of LASCO-C3 (up to 32 $R_{\odot} \sim 0.15$ AU), which yielded the first reported white-light observations of CME – CME interaction (Gopalswamy *et al.*, 2001). Although the interaction of successive CMEs at distances beyond the LASCO-C3 field of view can often be deduced from their white-light time-distance track or from radio emissions (Reiner, Kaiser, and Bougeret, 2001), only a few articles focused on the analysis of direct interaction following this first report (Reiner *et al.*, 2003). In the meantime, there had been a resurgence of interest regarding CME – CME interaction based on the analysis of *in situ* measurements near L1 (Burlaga, Plunkett, and St. Cyr, 2002; Burlaga *et al.*, 2003; Wang, Wang, and Ye, 2002; Wang, Ye, and Wang, 2003; Wang *et al.*, 2003a).

Reported observations became relatively routine with the development of heliospheric imaging, first with SMEI starting in 2003, and second with the HIs onboard STEREO starting in 2007 (see Figure 7 for some examples). Although a number of SMEI observations focused on series of CMEs (Bisi *et al.*, 2008; Jackson *et al.*, 2008), their analyses did not dwell on the physical processes occurring during CME – CME interaction. However, one of the very first CMEs observed remotely by STEREO was in fact a series of two interacting CMEs (Harrison *et al.*, 2009; Lugaz *et al.*, 2008, 2009; Lugaz, Vourlidas, and Roussev, 2009; Odstrcil and Pizzo, 2009; Webb *et al.*, 2009). During the period from the first remote detection in 2001 to routine remote observations in the late 2000s, numerical simulations have been used to fill the gap between the upper corona and the near-Earth space. Early simulations include the work by Wu, Wang, and Gopalswamy (2002), Odstrcil *et al.* (2003) and Schmidt and Cargill (2004). In the past decade, the combination of these three approaches (remote observations, *in situ* measurements, and numerical simulations) has resulted in a much deeper understanding of the physical processes occurring during CME – CME interaction.

4.1. Changes in the CME Properties

One of the essential aspects of CME – CME interaction is the change in CME properties, such as their speed, size, and expansion rate. This may directly affect space weather forecasting, as not only the CME speed and direction may change (modifying the hit/miss probability and the expected arrival time), but also its internal magnetic field (modifying the expected geomagnetic responses). In addition, understanding how CME – CME interaction changes CME properties can deepen our understanding of the internal structure of CMEs.

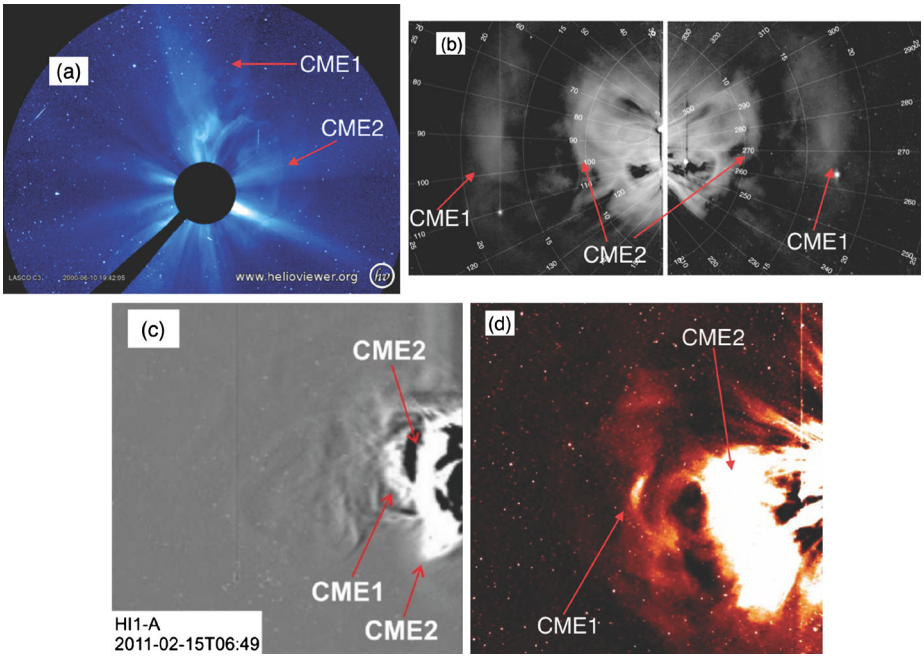

Figure 7 Observations of CME – CME interaction in LASCO-C3 and STEREO/HI1 fields of view. (a) Two CMEs from the initial report of CME – CME interaction by Gopalswamy *et al.* (2001). (b) Base-difference images on 25 May 2010 at 01:29UT (left: HI1A, right: HI1B) corresponding to the event studied in Lugaz *et al.* (2012). (c) Running-difference HI1A image of the event of 15 February 2011 studied in Temmer *et al.* (2014). (d) Base-difference image of the HI1A image of the 10 November 2012 event studied by Mishra, Srivastava, and Chakrabarty (2015). (c) Reproduced by permission of the AAS.

Many studies have investigated the change in the speed of CMEs due to their interaction, both through remote observations and numerical simulations. Some studies have focused on the nature of the collision, in terms of restitution coefficient and inelastic *vs.* elastic *vs.* super-elastic collision (Shen *et al.*, 2012a; Mishra, Srivastava, and Chakrabarty, 2015; Mishra, Srivastava, and Singh, 2015; Colaninno and Vourlidas, 2015; Mishra, Wang, and Srivastava, 2016). Different natures of collision seem to be possible (see for example the review by Shen *et al.*, 2017). Particularly if CME – CME collision can be super-elastic, it raises the questions of which circumstances yield an increase in total kinetic energy, and what the source of the kinetic energy gain is. However, CMEs are large-scale magnetized plasma structures propagating in the solar wind, and therefore the collision of CMEs is a much more complex process than the classic collision of ordinary objects. There are many factors causing the complexity: 1) depending on the speed of the CMEs, the interaction between two CMEs may involve zero, one, or two CME-driven shocks, some of which may dissipate during the interaction, 2) the interaction should take at least one Alfvén crossing time of a CME. With a typical CME size at 0.5 AU of 20 – 25 $R_{\odot}$ and a typical Alfvén speed inside a CME of 200 – 500 km s^{-1}, the interaction should take 8 – 24 hours, 3) the CME speed can change significantly, even at large distances from the Sun due to their interaction with the solar wind (Temmer *et al.*, 2011; Wu *et al.*, 2016), and 4) CME – CME interaction is inherently a 3D process and the changes in kinematics may differ greatly depending on the CME part that is considered (Temmer *et al.*, 2014). Using numerical simulations, it is somewhat possible to control some of these effects, for

example by performing simulations with or without interaction but identical CME properties and by knowing the velocity field in the entire 3D domain (Shen *et al.*, 2013c; Shen *et al.*, 2016). This has revealed that the momentum exchange with the ambient solar wind during CME – CME interaction may be neglected in some cases.

As CME – CME interaction involves a faster second CME overtaking a slower leading CME, the end result is to homogenize the speed, as was noted from *in situ* measurements in Burlaga, Plunkett, and St. Cyr (2002), Farrugia and Berdichevsky (2004), and through simulations by Schmidt and Cargill (2004) and Lugaz, Manchester, and Gombosi (2005), among others, and this occurs independently of the relative speed of the two CMEs. One main issue is to understand what determines the final speed of the complex ejecta that was formed through the CME – CME interaction. In an early work, Wang *et al.* (2005) found that in the absence of CME-driven shock waves, the final speed is determined by that of the slower ejecta, whereas Schmidt and Cargill (2004) and Lugaz, Manchester, and Gombosi (2005) found that when the CMEs drive shocks, the final speed is primarily determined by that of the faster ejecta, as the shocks propagation through the first magnetic ejecta accelerates it to a speed similar to that of the second ejecta (see Figure 8).

Most recent works have combined remote observations and numerical simulations. It now appears relatively clear that the final speeds depend on the relative masses of the CMEs, as well as on their approaching speed (Shen *et al.*, 2016), and, hence on their relative kinetic energy. Poedts *et al.* (2003) noted based on 2.5D simulations that the acceleration of the first CME increases as the mass of the second CME increases and that an apparent acceleration of the first CME is in fact due to a slower-than-expected deceleration. Making the situation more complex are the changes in the CME expansion during the propagation, as well as the fact that remote observations can be used to determine the velocity of the dense structures, but not really that of the low-density magnetic ejecta. As discussed in Lugaz, Manchester, and Gombosi (2005) and further in Lugaz, Vourlidas, and Roussev (2009), when the trailing shock impacts the leading magnetic ejecta, the dense sheath behind the shock must remain between the two magnetic ejecta, even as the shock propagates through the first ejecta. As HIs observe density structures, the observations may not be able to capture the shock propagating through a low-density ejecta.

In addition to changes in velocity, CME – CME interaction may result in the deflection of one CME by another (Xiong, Zheng, and Wang, 2009; Lugaz *et al.*, 2012; Shen *et al.*, 2012a). Combining these works, it appears that the deflection can reach up to 15° when the two CMEs are initially about 15 – 20° apart. Such angular separations are quite frequent between successive CMEs, as it corresponds to a delay of about one day for two CME originating from the same active region (due to solar rotation). This change in direction must be taken into account when deriving the changes in velocity, as done in Shen *et al.* (2012a) and Mishra, Wang, and Srivastava (2016).

Next, we discuss the changes in the CME internal properties, such as radial extent, radial expansion speed, and magnetic field strength. Only the radial extent can be reliably derived from remote observations (Savani *et al.*, 2009; Nieves-Chinchilla *et al.*, 2012; Lugaz *et al.*, 2012). Numerical simulations and remote observations both confirm that the leading CME stops expanding in the radial direction during the main phase (*i.e.* when the speed of both CMEs changes significantly) of interaction (Schmidt and Cargill, 2004; Lugaz, Manchester, and Gombosi, 2005; Xiong *et al.*, 2006; Lugaz *et al.*, 2012, 2013), and this behavior is typically associated with a "pancaking" of the leading CME (Vandas *et al.*, 1997). It should be noted that it appears nearly impossible for the CME radial extent to decrease, but rather the compression of the back of the leading CME is associated with a slowing down of its radial expansion. Lugaz, Manchester, and Gombosi (2005) discussed

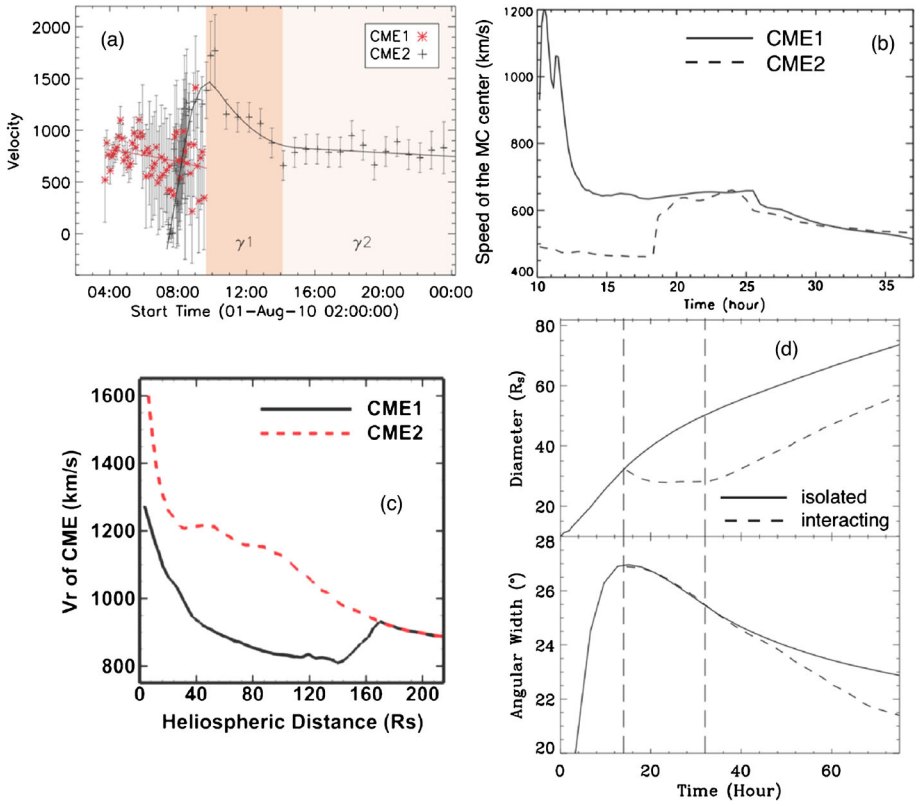

Figure 8 Changes in the CME properties due to CME – CME interaction. (a) Changes in speed associated with the August 2010 events from Temmer *et al.* (2012); see also Liu *et al.* (2012). (b) and (c): Change of speeds for simulated CMEs from the work of Lugaz, Manchester, and Gombosi (2005) and Shen *et al.* (2012b), respectively. (d) Change in radial size and angular width for a case with a shock overtaking a CME (dash) *vs*. an isolated CME (solid) from Xiong *et al.* (2006). (a) and (b): Reproduced by permission of AAS. (c) and (d): Reproduced by permission of John Wiley and Sons.

that the shock propagation through the leading CME is the main way in which the expansion slows. It is as yet unclear whether the compression changes for cases with or without shocks. What clearly changes is the resulting expansion of the leading CME after the end of the main interaction phase (*i.e.* after the shock exited the ejecta). Xiong *et al.* (2006) found that the leading CME overexpands to return to its expected size; as such, the compression is only a temporal state. This was confirmed by the statistical study of the magnetic ejecta radial size at different distances (Gulisano *et al.*, 2010), as well as one study where remote observations indicated compression, but a day after the interaction ended, when the CME impacted Earth, the *in situ* measurements indicated a typical CME size (Lugaz *et al.*, 2012). In numerical simulations with two magnetic ejecta (see Figure 9), the rate of overexpansion is found to depend on the rate of reconnection between the two ejecta; as such, it depends on the relative orientation of the two magnetic ejecta (Schmidt and Cargill, 2004; Lugaz *et al.*, 2013), but probably also on their density. The potential full coalescence of two ejecta into one was discussed in a few studies (Odstrcil *et al.*, 2003; Schmidt and Cargill, 2004; Chatterjee and Fan, 2013), but has not been investigated in detail with realistic reconnection rates.

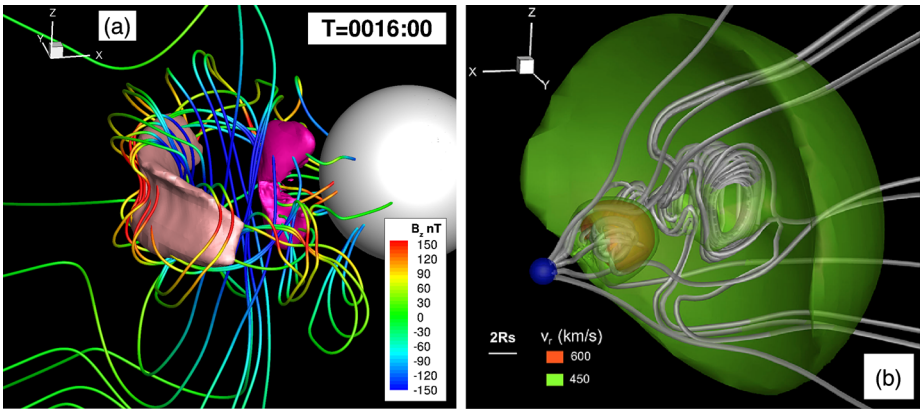

Figure 9 3D MHD simulations of CME – CME interaction. (a) Case simulated by Lugaz *et al.* (2013) with two CMEs with perpendicular orientations. 3D magnetic field lines are color-coded with the north-south B_z component of the magnetic field. Isosurfaces show regions of east-west B_y component of the magnetic field equal to ± 170 nT (pink positive, fuchsia negative). The CME fronts are at about 0.3 and 0.15 AU. (b) Simulation of Shen *et al.* (2013c) with isosurfaces of radial velocity and magnetic field lines in white. (b) Reproduced by permission of John Wiley and Sons.

4.2. Changes in the Shock Properties

In addition to changes in the CME properties, the fast forward shocks propagating inside the magnetic ejecta encounter highly varying and unusual upstream conditions, affecting the shock properties. Most of what is known about the changes in shock properties was learnt from numerical simulations; however, there have been many reported detections of shocks propagating inside a magnetic cloud or magnetic ejecta at 1 AU (Wang *et al.*, 2003a; Collier, Lepping, and Berdichevsky, 2007; Richardson and Cane, 2010a; Lugaz *et al.*, 2015b, 2016).

Vandas *et al.* (1997) noted that a shock propagates faster inside a magnetic cloud because of the enhanced fast magnetosonic speeds inside, which may result in shock – shock merging close to the nose of the magnetic cloud but two distinct shocks in the flanks. Odstrcil *et al.* (2003) noted that associated with this acceleration, the density jump becomes smaller. Lugaz, Manchester, and Gombosi (2005) performed an in-depth analysis of the changes in the shock properties, dividing the interaction into four main phases: i) before any physical interaction, when the shock propagates faster than an identical isolated shock because of the lower density in the solar wind, ii) during the shock propagation inside the magnetic cloud, when the shock speed in a rest frame increases and its compression ratio decreases, confirming the findings of Odstrcil *et al.* (2003), iii) during the shock propagation inside the dense sheath when the shock decelerates, as pointed out by Vandas *et al.* (1997), and iv) the shock – shock merging, when as predicted by MHD theory, a stronger shock forms followed by a contact discontinuity. If the shock is weak or slow enough, it may dissipate as it propagates into the region of higher magnetosonic speed inside the magnetic cloud (Xiong *et al.*, 2006; Lugaz *et al.*, 2007). High spatial resolution is necessary to resolve weak shocks in MHD simulations, and low resolution may affect the prediction of shock dissipation. The merging or dissipation of shocks was noted by Farrugia and Berdichevsky (2004), when *Helios* measured four shocks at 0.67 AU and ISEE-3 measured only two shocks later on at 1 AU. Shock – shock interaction was studied by means of 2D MHD simulations by Poedts *et al.*

(2003), where the authors identified a fast forward shock and a contact discontinuity as the result of two fast forward shocks merging.

4.3. Cases Without Direct Interaction

In a similar way that the succession but not the interaction *per se* of CMEs can affect the resulting flux of SEPs, the succession of CMEs, even without interaction, may affect the properties of the second (and subsequent) CMEs. Lugaz, Manchester, and Gombosi (2005) performed the simulation of the two CMEs, initiated with the same parameters (initial energy, size, orientation, *etc.*) 10 hours apart. The second CME did not decelerate as much as the first and therefore had a faster speed and a faster shock wave, even before the interaction started. This result was confirmed in studies with different orientations (Lugaz *et al.*, 2013). Many of the shortest Sun-to-1 AU transit times of CMEs appear to be associated with a succession of non-interacting CMEs. It has been suggested that this was the case of the Carrington event of 1859 (Cliver and Svalgaard, 2004), the Halloween events of 2003 (Tóth *et al.*, 2007), and the 23 July 2012 event (Liu *et al.*, 2014a), each of which is a case where the propagation lasted less than 20 hours, *i.e.* the average transit speed was in excess of 2000 $\mathrm{km\,s^{-1}}$. Note that only 15 events propagated from Sun to Earth in less than 24 hours in the past 150 years (Gopalswamy *et al.*, 2005). Liu *et al.* (2014a) and Liu *et al.* (2015) proposed that this succession of non-interacting CMEs may produce a "perfect storm" with the most extreme geoeffectiveness. A careful analysis of which situation results in the most geoeffective storms has to be undertaken. The main reason for this reduced deceleration is that the first CME removed some of the ambient solar wind mass, resulting in less dense and faster flows ahead of the subsequent CME. As such, the second CME experiences less drag and propagates faster (Lugaz, Manchester, and Gombosi, 2005; Liu *et al.*, 2014a; Temmer and Nitta, 2015).

4.4. Resulting Structures

The complex interaction between different shock waves and magnetic ejecta can result in a variety of structures at 1 AU. The "simplest" resulting structure is a multiple-magnetic cloud (multiple-MC) event (Wang, Wang, and Ye, 2002), in which a single dense sheath precedes two (or more) distinct MCs (or MC-like ejecta). The two MCs are separated by a short period of large plasma β, corresponding to hot plasma with a weaker and more turbulent magnetic field (Wang, Ye, and Wang, 2003), which may be an indication of reconnection between the ejecta (see Figure 10a). Typically, both MCs have a uniform speed profile, *i.e.* they propagate approximately with the same speed. The prototypical example of a multiple-MC event is the 31 March – 1 April 2001 multiple-MC event (Wang, Ye, and Wang, 2003; Berdichevsky *et al.*, 2003; Farrugia *et al.*, 2006a). Such structures have been successfully reproduced in simulations (Wang *et al.*, 2005; Lugaz, Manchester, and Gombosi, 2005; Xiong *et al.*, 2007; Shen *et al.*, 2011). These simulations reveal that the dense sheath ahead of the two MCs may be the result of the merging of two shock waves. In this case, it is expected that the sheath may be composed of a leading hot part (the sheath of the new merged shock) followed by a denser and cooler section (material that has been compressed twice, see Lugaz, Manchester, and Gombosi, 2005). The extremely dense sheath preceding the March 2001 event may be related to a shock – shock merging. It is also possible that the shock driven by the overtaking CME dissipates as it propagates inside the first MC, which would also result in a single sheath preceding two MCs.

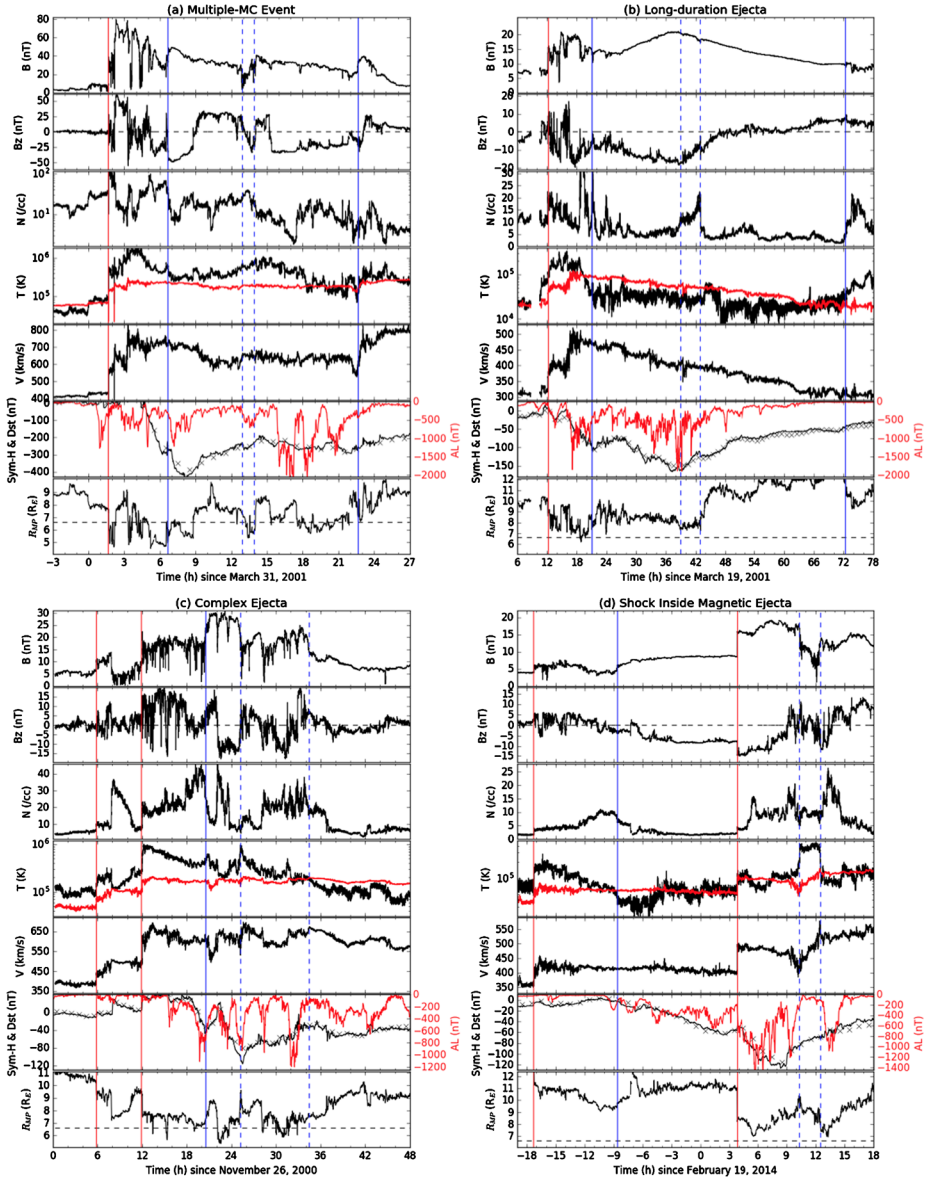

Figure 10 *In situ* measurements of CME – CME interaction. The panels show the magnetic field strength, B_Z component in Geocentric Solar Magnetospheric (GSM) coordinates, proton density, temperature (expected temperature in red), velocity, Sym-H index (Dst with crosses, AL in red), and dayside magnetopause minimum location following Shue *et al.* (1998), from top to bottom. Shocks are marked with red lines and CME boundaries with blue lines (dashed for internal boundaries).

Multiple-MC events correspond to cases when the individual MCs can be distinguished, although the uniform speed and the single sheath indicate that they interacted. When multiple ejecta cannot be distinguished, the resulting structure is typically referred to as a complex ejecta or compound stream (Burlaga *et al.*, 2003). These structures often have a decreasing

speed profile, typical of a single event, but with complex magnetic fields and a duration of several days (see Figure 10c). Such complex streams may be caused by a number of factors, including: 1) interaction close to the Sun, resulting in quasi-cannibalism (Gopalswamy *et al.*, 2001), 2) the relative orientation of the successive ejecta favorable for reconnection (Lugaz *et al.*, 2013), or 3) interaction between more than two CMEs (Lugaz *et al.*, 2007). Some events, for example the event of 26 – 28 November 2000, which involved between three and six successive CMEs, have been analyzed as multiple-MC event (Wang, Wang, and Ye, 2002) or complex ejecta (Burlaga, Plunkett, and St. Cyr, 2002). Even if individual ejecta can be distinguished, they are of short duration (for this event, between 3 and 8 hours), and the magnetic field is not smooth. In the simulation of Lugaz *et al.* (2007), it was found that the complex interaction of three successive CMEs and the associated compression resulted in a period of enhanced magnetic field and higher speed at 1 AU, but without individual ejecta being identifiable. In this sense, complex ejecta at 1 AU are similar to merged interaction regions that are often measured in the outer heliosphere, corresponding to the merging of many successive CMEs (Burlaga, Ness, and Belcher, 1997; le Roux and Fichtner, 1999). It is also possible that the interaction between a fast and massive CME and a slow and small CME may result in cannibalism, whereas interaction of CMEs with similar size and energy results in a multiple-MC event. Numerical simulations have focused primarily on the interaction of CMEs of comparable energies and sizes, but a more complete investigation of the effect of different initial sizes and CME energies is required, building upon the work of Poedts *et al.* (2003).

It has also been proposed that seemingly isolated but long-duration events (events that last 36 hours or more at 1 AU) may be associated with the interaction of successive CMEs of nearly perpendicular orientation (see Figure 10b). Dasso *et al.* (2009) performed the analysis of the 15 May 2005 CME, including *in situ* measurements, radio emissions, and remote observations (Hα, EUV, magnetograms, and coronagraphic data). They concluded that this large event, which lasted close to 2 days at 1 AU, was likely to be associated with two non-merging MCs, of nearly perpendicular orientation. The simulations of Lugaz *et al.* (2013) included a case in which two CMEs were initiated with near-perpendicular orientation, as well as two CMEs with the same initial orientation. In the latter case, the authors found that a multiple-MC event was the resulting structure; in the former case, the resulting structure was a long-duration transient having many of the characteristics of a single ejecta. Lugaz and Farrugia (2014) compared the results at 1 AU of this simulation with the 19 – 22 March 2001 CME, another 48-hour period of smooth and slowly rotating magnetic field, monotonically decreasing speed, and lower-than-expected temperature. In both the simulation and data, the second part of the event was characterized by a nearly unidirectional magnetic field. The difference between complex ejecta and this type of transient lies in the smoothness of the magnetic field. Both the events studied by Dasso *et al.* (2009) and Lugaz and Farrugia (2014) have been characterized as a single isolated CME, but their size (twice larger than a typical MC) and the variation of the magnetic field make it unlikely.

These three cases (multiple-MCs, complex ejecta, and long-duration events) correspond to full interaction, in the sense that the resulting structure at 1 AU is propagating with a single-speed profile (typically monotonically decreasing). The main examples of partial ongoing interaction are associated with the propagation of a fast forward shock wave inside a preceding ejecta (Wang *et al.*, 2003a; Collier, Lepping, and Berdichevsky, 2007; Lugaz *et al.*, 2015b). There is a clear difference between the part of the first CME that has been accelerated by the overtaking shock as compared to its front, which is still in "pristine" conditions (see Figure 10d). In some cases, the back of the first CME is in the process of merging with the front of the second CME (Liu *et al.*, 2014b), *i.e.* a complex ejecta or a

long-duration event is in the process of forming. In the study of Lugaz *et al.* (2015b), the authors identified 49 such shocks propagating within a previous magnetic ejecta between 1997 and 2006. Most such shocks occur toward the back of the ejecta, and shocks tend to be slower as they approach the CME front. This can be interpreted as an indication that a number of shocks dissipate inside a CME before exiting it. The two main reasons are that CMEs tend to be expanding and have a decreasing speed profile and that the peak Alfvén speed typically occurs close to the center of the magnetic ejecta. The latter reason means that shocks become weaker as they approach the center of the ejecta. The former reason implies that shocks propagate into increasingly higher upstream speeds as they move from the back to the front of the CME. Lugaz *et al.* (2015b) reported cases when the speed at the front of the first CME exceeds the speed of the overtaking shock, *i.e.* because of the CME expansion, the shock cannot overtake the front of the CME.

These four different structures, often observed at 1 AU, represent four different ways for CME – CME interaction to affect our geospace in a way that differs from the typical interaction of a CME with Earth's magnetosphere. We give some details on the geoeffectiveness of these structures in the following section.

5. The Geoeffectiveness of Interacting CMEs

Compared to isolated ejecta, the geomagnetic disturbances brought about by interacting CMEs need to account for the changes in parameters resulting from their interaction. These typically, although not always, enhance their geoeffectiveness. Individual CMEs and their subset, magnetic clouds (Burlaga *et al.*, 1981), are known to be major sources of strong magnetospheric disturbances (Gosling *et al.*, 1991). This is mainly because they often contain a slowly varying negative north-south (B_z) magnetic field component that can reach extreme values (see, *e.g.*, Farrugia *et al.*, 1993; Tsurutani *et al.*, 1988). The passage of ejecta at 1 AU takes typically about one day, which means that these disturbances can last for many hours. By contrast, passage of interacting ejecta as well as complex ejecta can take $\sim$3 days at 1 AU (Burlaga, Plunkett, and St. Cyr, 2002; Xie *et al.*, 2006), so that the magnetosphere is under strong solar wind forcing for a much longer time. Below we show an example of a storm where the Dst index, which monitors the strength of the ring current, remained below -200 nT for about 21 hours. Thus from the point of view of space weather, CME – CME interactions are key players.

Clearly, to assess the overall impact of ejecta interactions on space weather, it is crucial to determine how frequently they occur at 1 AU. Some studies have addressed this issue. Examining the causes of major geomagnetic storms in the 10-year period 1996 – 2005, Zhang *et al.* (2007) showed that at least 27% of the intense storms (over 88 storms from 1997 to 2005) were due to multiple CMEs. Using a different approach, Farrugia *et al.* (2006b) used the epsilon parameter from Akasofu (1981) to define so-called "large events". They used this parameter to estimate the energy extracted by the magnetosphere from the solar wind and the powering of the magnetosphere by the solar wind. In the period 1995 – 2003, they found that 6 out of the 16 largest events ($\sim$37%) involved CMEs interacting with each other to form complex ejecta. One may conclude that CME – CME interactions are important drivers of extreme space weather. Indeed, some recent studies using multi-spacecraft observations at different radial distances and wide azimuthal separations have been undertaken to illustrate how these interactions play a leading role. A case in point are the interplanetary and geomagnetic consequences of multiple solar

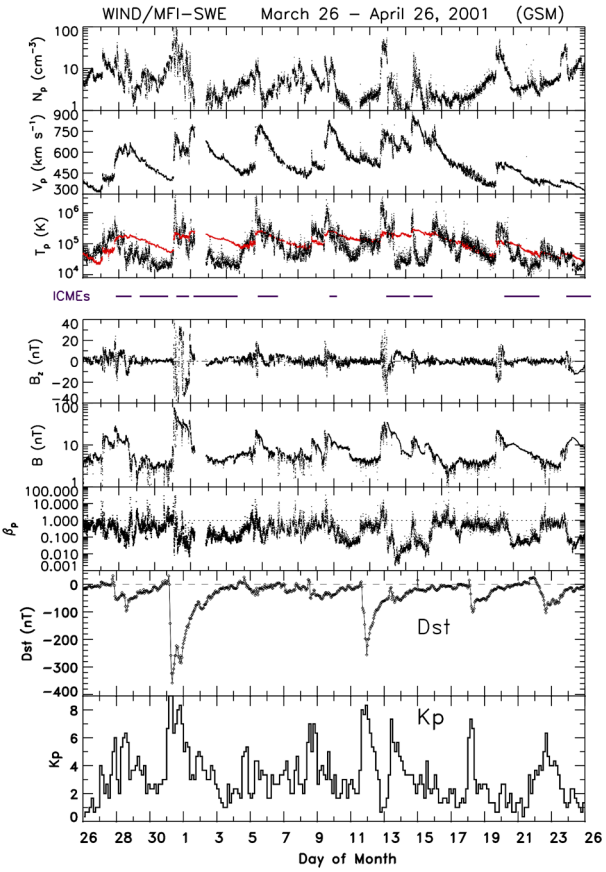

Figure 11 Solar wind measurements and geomagnetic indices of a 31-day period in March – April 2001. The panels show from top to bottom the proton density, bulk speed, temperature (expected temperature in red), the 11 ICMEs identified in this period, the B_Z component of the magnetic field (in GSM coordinates), the total magnetic field, the proton β, the storm-time Dst index, and the planetary Kp index.

eruptions that took place on 1 August 2010 (Möstl *et al.*, 2012; Temmer *et al.*, 2012; Liu *et al.*, 2012).

CME – CME interactions are more frequent during solar maximum conditions when the number of CMEs erupting from the Sun may reach half a dozen *per* day. As an illustration, Figure 11 shows *in situ* measurements by *Wind* of a 31-day period during the maximum phase of Solar Cycle 23. From top to bottom, the figure shows the proton density, bulk speed, temperature, the 11 ICMEs identified in this period (from Richardson and Cane, 2010b), the B_z component of the magnetic field (in GSM coordinates), the total field, the proton β, the storm-time Dst index, and the planetary Kp index. The red trace in the third panel from the top shows the expected proton temperature for normal solar wind expansion (Lopez, 1987). It can be seen that the measured temperature is often well below this value. This is an often-used indicator of ejecta material in space (following the initial report by Gosling, Pizzo, and Bame, 1973, used to select CMEs by Richardson and Cane, 1993, 1995). Complementary to this are the episodic high magnetic field strengths. The sawtooth appearance of the temporal profile of the bulk speed indicates a series of radially expanding transients.

With so many CMEs, this interval represents a particularly active period at the Sun and in the inner heliosphere (see Wang, Ye, and Wang, 2003; Berdichevsky *et al.*, 2003). Correspondingly, the geomagnetic Kp index and the storm-time Dst index indicate that it is also a very disturbed period for the magnetosphere. The event on 31 March – 1 April 2001 stands

out. Here the proton density, the amplitude of the B_z component of the magnetic field, and the magnetic field strength all reach the highest values during this whole interval. The Dst index (uncorrected for magnetopause currents, see below) reaches peak values of -350 nT and has a two-pronged profile, and the Kp index saturates (Kp = 9).

The strong geomagnetic effects of partial or total ejecta mergers may be considered to result from a combination of two effects; on top of the geoeffectiveness of the individual ejecta there is the effect introduced by the interaction process. Data and simulations have elaborated on aspects of CME – CME interactions that enhance their geoeffectivness. Berdichevsky *et al.* (2003) and Farrugia and Berdichevsky (2004) noted the following features: (i) transfer of momentum of the trailing shock and its post-shock flow to the leading CME, (ii) acceleration (deceleration) of the leading (trailing) CME, (iii) strengthening of the shock after its merger with the trailing shock, and (iv) heating and compression of the leading ejecta. In simulations, Lugaz, Manchester, and Gombosi (2005) emphasized the importance of the trailing shock as it passes through the preceding ejecta to eventually merge with the leading shock, strengthening it. Below, we first give an example of the role of the enhanced density in intensifying the geomagnetic disturbances and then discuss another example where the role of the trailing shock is central.

The geomagnetic storm during the event on 31 March – 1 April 2001 (Figure 10a) has been studied by many researchers. Most relevant here is that Farrugia *et al.* (2006a) argued that the extreme severity of the storm was ultimately due to a very dense plasma sheet combined with strong southward magnetic fields. They showed that the plasma sheet densities were, in turn, correlated with the high densities in the merged ejecta. Since compression of plasma is a feature of CME – CME interactions, the authors concluded that the interaction was ultimately responsible for causing this super-storm, with Dst reaching values below -250 nT for several hours.

We illustrate this in Figure 12. The middle panel gives the total magnetic field for reference and shows the two interacting ejecta in the process of merging. In the top panel we plot the density of the interacting ejecta (thick black trace). Below in color is the density of the plasma sheet obtained from the total ion densities above ~ 100 eV acquired by three Los Alamos National Laboratory (LANL) spacecraft in geostationary orbit on the nightside (18-06 MLT). Below, we show this density again as a single-valued function (divided by four for clarity). To produce this, all data were retained where there was no overlap between measurements from the different spacecraft. When there was an overlap, we kept only data acquired closest to local midnight. One can see that the temporal trends in the densities of the plasma sheet (N_{ps}) and the ejecta (N_{sw}) are very similar. The bottom panel shows a scatter plot of N_{ps} *vs.* N_{sw}, for which the regression line gives $N_{ps} \sim N_{sw}^{1/2}$.

The strength of the ring current depends mainly on two factors: (i) the electric field in which the particles drift as they travel inwards from the plasma sheet, and (ii) the density of the plasma sheet itself, since it constitutes the seed population (Jordanova *et al.*, 2006). In this case, we have a large enhancement of the latter. Using the global kinetic drift-loss model developed by Jordanova *et al.* (1996), it was shown that the two-dip Dst profile could be reproduced even when the code was run with the plasma sheet density kept constant at its original value. However, the intensity of the storm was thereby grossly underestimated. It could be adequately reproduced only when the plasma sheet density was updated in accordance with the data (see Figure 4 in Farrugia *et al.*, 2006a). The result was a storm where Dst stayed below -200 nT for 21 hours and below -250 nT for 7 hours. In a broader context, Borovsky, Thomsen, and Elphic (1998) carried out a statistical study relating properties of the plasma sheet with those of the solar wind. One of these was the density, where they found a strong correlation. The relationship they obtained, with N_{ps} scaling as the square root of

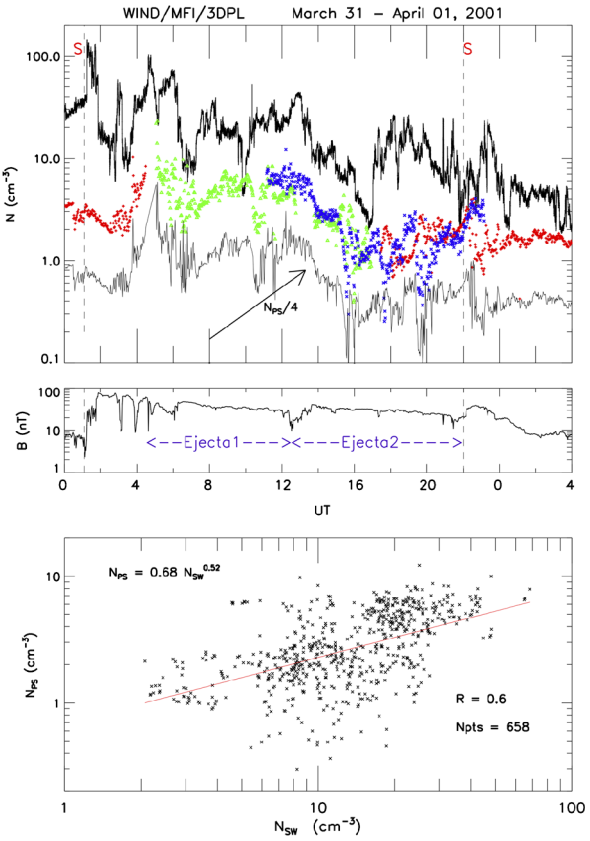

Figure 12 Comparison of the solar wind and plasma sheet densities during the 31 March – 1 April 2001 CME – CME interaction event. The top panels show the solar wind density (thick black line), total ion densities above ~ 100 eV acquired by three Los Alamos National Laboratory (LANL) spacecraft in geostationary orbit on the nightside in colored symbol, and the compound plasma sheet density (divided by four for clarity). The middle panel shows the total magnetic field. The bottom panel shows a scatter plot of N_{ps} *vs.* N_{sw} and a best-fit line. Adapted from Farrugia *et al.* (2006a) and published by permission of John Wiley and Sons.

N_{sw}, is similar to that described here. However, compared to their survey, the dynamic range of the density in the case just described was a factor of five higher.

An important implication is that CME – CME interaction can be a viable source of two-dip geomagnetic storms. Kamide *et al.* (1998) studied over 1200 geomagnetic storms and noted that a significant proportion of these were double-dip storms; the Dst index reaches a minimum, recovers for a few hours, and then reaches a second minimum. A traditional view of how this profile comes about is the sheath-ejecta mechanism, that is, the negative B_z fields in the sheath region, which have been compressed by the shock ahead of the ejecta, are responsible for the first Dst drop and the negative B_z phase in the ejecta is then responsible for the second drop (Tsurutani *et al.*, 1988; Gonzalez *et al.*, 2002, and the review by Tsurutani and Gonzalez, 1997). Here we have given an example of how such two-dip Dst profiles can arise from CME – CME interactions. In a wide survey of major storms (Dst < -100 nT) over Solar Cycle 23 (1996 – 2006), Zhang, Richardson, and Webb (2008) found that a common source of double-dip storms consists of closely spaced or interacting CMEs. Of course, there are other levels of complexity, such as multiple-dip storms (see for example, Xiong *et al.*, 2006 and Zhang, Richardson, and Webb, 2008 and Richardson and Zhang, 2008).

We so far primarily discussed cases corresponding to multiple-MC events or two (or more) CMEs in close succession that do not interact, however. Lugaz and Farrugia (2014) discussed how a long-duration seemingly isolated event resulting from the merging of two CMEs may drive the magnetosphere for a long period, resulting in sawtooth events associ-

ated with injection of energetic particles observed at a geosynchronous orbit. In the case of the 19 – 22 March 2001 event (see Figure 10b), in addition to sawtooth events, it resulted in an intense geomagnetic storm whose peak Dst reached −149 nT and which remained below the moderate level (below −50 nT) for 55 hours.

We now consider a case where the trailing shock passing through the front CME plays a leading role in the resulting geomagnetic disturbances. There are two effects of the interaction on increasing geoeffectiveness. First, the leading ejecta are compressed by either the overtaking shock or magnetic ejecta, or a combination of both (Burlaga, Hewish, and Behannon, 1991; Vandas *et al.*, 1997; Farrugia and Berdichevsky, 2004; Lugaz, Manchester, and Gombosi, 2005; Xiong *et al.*, 2006; Liu *et al.*, 2012). Assuming conservation of magnetic flux, the compressed southern B_z interval is more geoeffective than the uncompressed southern B_z interval (see the quantitative analysis in Wang *et al.*, 2003c and Xiong *et al.*, 2007). Second, the overtaking shock itself and the sheath of compressed ejecta may be more efficient in driving geoeffects. Recently, Lugaz *et al.* (2015b) and Lugaz *et al.* (2016) published survey studies about the effect of a shock propagating inside a preceding ejecta on the geoeffectiveness of the shock/sheath region. They found that about half the shocks whose sheaths results in at least a moderate geomagnetic storm are shocks propagating within a previous CME or a series of two shocks. Shocks inside CMEs, as a potential source of intense geomagnetic storms, were also discussed by Wang *et al.* (2003a) and further investigated in Wang *et al.* (2003b). Specific examples were also discussed in Lugaz *et al.* (2015a), who argued that the combination of a high dynamic pressure and a compressed magnetic field just behind the shock may be particularly efficient in pushing Earth's magnetopause earthward, and therefore in driving energetic electron losses in Earth's radiation belt. An example of such an event is given in Figure 10d for a shock inside a magnetic ejecta that occurred on 19 February 2014 and resulted in an intense geomagnetic storm.

As a result of their complex and turbulent magnetic field and the short duration of any southward periods, complex ejecta often result in strong but not extreme driving of Earth's magnetosphere. For example, the 26 – 28 November 2000 event (Figure 10b), caused by a series of homologous CMEs as discussed in Section 2.2, resulted in a peak Dst of −80 nT between 26 and 28 November, even though the dawn-to-dusk electric field reached values above 10 $\mathrm{mV\,m^{-1}}$, typically associated with intense geomagnetic storms. The large and rapid changes in the orientation of the magnetic field certainly played a role in the reduced geoeffectiveness (Burlaga, Plunkett, and St. Cyr, 2002; Wang, Wang, and Ye, 2002; Lugaz *et al.*, 2007).

The response of the magnetosphere is expected to become nonlinear and even saturate under the strong forcing when interacting ejecta pass Earth, for example, the polar cap potential (Hill, Dessler, and Wolf, 1976; Siscoe, Crooker, and Siebert, 2002) and erosion of the dayside magnetosphere (Mühlbachler *et al.*, 2005). Furthermore, the correction to the raw Dst index from magnetopause currents (Chapman–Ferraro currents, Burton, McPherron, and Russell, 1975) becomes inappropriate since the high-latitude auroral Birkeland currents (so called, Region 1 currents) have taken over the role of the Chapman–Ferraro currents in standing off the solar wind (Siscoe, McPherron, and Jordanova, 2005, and references therein). Following Vasyliūnas (2004) and Siscoe, McPherron, and Jordanova (2005), one can speak of the magnetosphere as having transitioned from being solar-wind-driven to being ionosphere-driven.

6. Discussions and Conclusion

We have reviewed the main physical phenomena and concepts associated with the initiation and interaction of successive CMEs, including their effects on particle acceleration and their

potential for strong driving of Earth's magnetosphere. Initiation mechanisms need to be studied in the photosphere and chromosphere by combining observations and simulations. The close relation between CMEs and filaments leads to the necessity for more detailed studies on filament evolution and partial eruptions that result in multiple CMEs (twin-CMEs, sympathetic CMEs, and homologous CMEs).

Homologous CMEs and sympathetic CMEs are two main sources of interacting CMEs, although unrelated successive CMEs may interact as well. Based on the current knowledge, the possible mechanisms of one CME triggering another include: (1) destabilization of magnetic structures by removing the overlying field, and (2) the continuous emergence of flux and helicity from the lower atmosphere. However, statistical studies have suggested that homologous or sympathetic CMEs only correspond to a small fraction of total CMEs, meaning that not all CMEs can trigger subsequent eruptions. This raises the serious question as to why some CMEs trigger another CME while others do not. Answering this question will directly determine the capability of forecasting of homologous and sympathetic CMEs. The coronal magnetic field is the key information in studying the initiation of CMEs. However, it is now mostly known from extrapolation methods based on limited observations. *Solar Orbiter*, to be launched in 2018, will provide the vector magnetic field at the photosphere from a point of view other than that of the Earth. Combined with the magnetic field observed by SDO, it may increase the accuracy of the coronal magnetic field extrapolation.

With respect to particle acceleration, it is clear that SEPs are strongly affected by preconditioning in terms of turbulence and seed population. Radio enhancements themselves are likely to be directly related to the CME – CME interaction process. SEPs, on the other hand, are more likely to be related to having a succession of (not necessarily interacting) CMEs. Enhanced levels of turbulence and suprathermal particles following a first CME are likely physical explanations. Studies have shown that type II radio burst intensification is due to the front of a faster second CME colliding with the rear of a slower preceding CME; but shock – streamer interaction is also a likely cause of such enhancements. In fact, enhanced type II radio signatures may occur for different types of interaction scenarios.

Wide-angle heliospheric imaging of CMEs, now routinely performed by STEREO, has resulted in a new era of study of CME – CME interaction where 3D kinematics can be combined with Sun-to-Earth imaging of succession of CMEs, 3D numerical simulations, and radio observations. Many of the recent studies have focused on the relation between the interaction and the resulting structure measured at 1 AU, as well as on the exchange of momentum between the CMEs. In many instances, the two CMEs are found to propagate after their interaction with a uniform speed profile, similar to that of an isolated CME, but how this final speed relates to that of the two CMEs before the interaction is still an area of active research. The "compression" of the leading CME (associated with a reduced rate of expansion) and the potential deflection of the CMEs are two additional effects of CME – CME interaction that can have a strong influence on space weather forecasting. The exchange of momentum between CMEs is likely to involve a series of phases, including compression of the leading CME by the trailing shock wave that increases the CME magnetic energy, followed by an overexpansion of the leading CME and potential reconnection between the two magnetic ejecta.

Most studies still primarily focus on the different aspects of CME – CME interaction (initiation, SEP acceleration, heliospheric interaction, *in situ* measurements, geoeffects) without attempting to obtain a global view. One issue is that heliospheric imaging provides information about different density structures and their kinematics, but not about the magnetic field. More global studies, for example, to determine whether sympathetic or homologous (or unrelated) eruptions are more likely to result in CME – CME interaction, and to which

structures at 1 AU they correspond are now possible with modern remote imaging but have not been undertaken yet. The study of SEP acceleration and radio bursts associated with successive CMEs must be combined with studies of the stereoscopic observations to determine the deprojected CME directions, distances, and kinematics, as done only for few events so far (Temmer *et al.*, 2014; Ding *et al.*, 2014b). Similar studies may help to investigate which time delay between successive CMEs results in the most intense geoeffects, and what the most extreme scenario can be. A recent investigation by the Cambridge Centre for Risk Studies of the economical consequences of an extreme CME took as its base scenario the impact in close succession of two non-interacting CMEs, similar to the perfect storm scenario of Liu *et al.* (2014a). It is as yet unclear if such a scenario would result in stronger magnetospheric, ionospheric, and ground currents as compared to two CMEs in the process of interacting (shock inside CME) or having interacted (multiple-MC event).

Although detailed investigations of CME – CME interaction became more frequent following the report by Gopalswamy *et al.* (2001) of a total disappearance of one CME following its overtaking by a faster CME (referred to as CME "cannibalism"), total magnetic reconnection might not take place regularly, as it might be too slow for effectively merging entire flux ropes. For this reason, the most common result of CME – CME interaction at 1 AU is multiple-MC events, where the individual ejection can be distinguished, complex ejecta where some of the individual characteristics are lost, and shocks propagating inside a previous CME. Each of these has a different way to interact with Earth's magnetosphere. Often, the long-duration driving and compressed magnetic fields result in intense geoeffects; in addition, shocks within CMEs have a higher probability of having a geoeffective sheath than shocks propagating into typical solar wind conditions.

Currently available *in situ* data show us only the consequences of CME – CME interaction, but not the interaction process itself. *In situ* data during the interaction process are needed, as was possible with *Helios* (Farrugia and Berdichevsky, 2004). *Solar Orbiter* and *Solar Probe+* will provide opportunities for measuring the interaction process as it occurs, and to determine the fate of shocks propagating inside ejecta, and the irreversibility (or not) of the interaction. Studies made possible by these spacecraft when they are in alignment (conjunction) will help us to answer some of these outstanding questions.

Acknowledgements We acknowledge the following grants: NASA grant NNX15AB87G and NSF grants AGS1435785, AGS1433213 and AGS1460179 (N. Lugaz), NSFC grants 41131065 and 41574165 (Y. Wang), Austrian Science Fund FWF: V195-N16 (M. Temmer), and NASA grant NNX16AO04G (C.J. Farrugia). N. Lugaz would like to acknowledge W.B. Manchester, I.I. Roussev, Y.D. Liu, G. Li, J.A. Davies, T.A. Howard, and N.A. Schwadron for fruitful discussion about CME – CME interaction over the years, as well as the VarSITI program. Some of the figures in this article have been published by permission of the AAS and John Wiley and Sons, as indicated in the text.

Disclosure of Potential Conflicts of Interest The authors declare that they have no conflicts of interest.

References

Akasofu, S.I.: 1981, *Space Sci. Rev.* **28**, 121. DOI.
Antiochos, S.K., DeVore, C.R., Klimchuk, J.A.: 1999, *Astrophys. J.* **510**, 485. DOI.
Aran, A., Lario, D., Sanahuja, B., Marsden, R.G., Dryer, M., Fry, C.D., *et al.*: 2007, *Astron. Astrophys.* **469**, 1123. DOI.
Arge, C.N., Pizzo, V.J.: 2000, *J. Geophys. Res.* **105**, 10465. DOI.
Bemporad, A., Zuccarello, F., Jacobs, C., Mierla, M., Poedts, S.: 2012, *Solar Phys.* **281**, 223. DOI.
Berdichevsky, D.B., Farrugia, C.J., Lepping, R.P., Richardson, I.G., Galvin, A.B., Schwenn, R., *et al.*: 2003, In: Velli, M., Bruno, R., Malara, F., Bucci, B. (eds.) *Solar Wind Ten*, *Amer. Inst. Physics Conf. Ser.* **679**, 758. DOI.

Biesecker, D.A., Thompson, B.J.: 2000, *J. Atmos. Solar-Terr. Phys.* **62**, 1449. DOI.
Bisi, M.M., Jackson, B.V., Hick, P.P., Buffington, A., Odstrcil, D., Clover, J.M.: 2008, *J. Geophys. Res.* **113**, 00. DOI.
Borovsky, J.E., Thomsen, M.F., Elphic, R.C.: 1998, *J. Geophys. Res.* **103**, 17617. DOI.
Bothmer, V., Posner, A., Kunow, H., Müller-Mellin, R., Herber, B., Pick, M., *et al.*: 1997, In: Wilson, A. (ed.) *Correlated Phenomena at the Sun, in the Heliosphere and in Geospace*, *ESA* **SP-415**, 207. ADS
Brown, D.S., Nightingale, R.W., Alexander, D., Schrijver, C.J., Metcalf, T.R., Shine, R.A., *et al.*: 2003, *Solar Phys.* **216**, 79. DOI.
Brueckner, G.E., Howard, R.A., Koomen, M.J., Korendyke, C.M., Michels, D.J., Moses, J.D., *et al.*: 1995, *Solar Phys.* **162**, 357. DOI.
Burlaga, L.F., Behannon, K.W., Klein, L.W.: 1987, *J. Geophys. Res.* **92**, 5725. DOI.
Burlaga, L.F., Hewish, A., Behannon, K.W.: 1991, *J. Geophys. Res.* **96**, 21. DOI.
Burlaga, L.F., Ness, N.F., Belcher, J.W.: 1997, *J. Geophys. Res.* **102**, 4661. DOI.
Burlaga, L.F., Plunkett, S.P., St. Cyr, O.C.: 2002, *J. Geophys. Res.* **107**, 1. DOI.
Burlaga, L., Sittler, E., Mariani, F., Schwenn, R.: 1981, *J. Geophys. Res.* **86**, 6673. DOI.
Burlaga, L., Berdichevsky, D., Gopalswamy, N., Lepping, R., Zurbuchen, T.: 2003, *J. Geophys. Res.* **108**, 2. DOI.
Burton, R.K., McPherron, R.L., Russell, C.T.: 1975, *J. Geophys. Res.* **80**, 4204. DOI.
Cane, H.V., McGuire, R.E., von Rosenvinge, T.T.: 1986, *Astrophys. J.* **301**, 448. DOI.
Cane, H.V., Reames, D.V., von Rosenvinge, T.T.: 1988, *J. Geophys. Res.* **93**, 9555. DOI.
Cargill, P.J.: 2004, *Solar Phys.* **221**, 135. DOI.
Chandra, R., Schmieder, B., Mandrini, C., Démoulin, P., Pariat, E., Török, T., Uddin, W.: 2011, *Solar Phys.* **269**, 83. DOI.
Chatterjee, P., Fan, Y.: 2013, *Astrophys. J. Lett.* **778**, 8. DOI.
Chen, P.F.: 2011, *Living Rev. Solar Phys.* **8**, 1. DOI.
Chen, P.F., Shibata, K.: 2000, *Astrophys. J.* **545**, 524. DOI.
Chen, C., Wang, Y., Shen, C., Ye, P., Zhang, J., Wang, S.: 2011, *J. Geophys. Res.* **116**, 12108. DOI.
Cheng, X., Zhang, J., Ding, M.D., Olmedo, O., Sun, X.D., Guo, Y., Liu, Y.: 2013, *Astrophys. J. Lett.* **769**, 25. DOI.
Cliver, E.W., Svalgaard, L.: 2004, *Solar Phys.* **224**, 407. DOI.
Cliver, E.W., Kahler, S.W., Reames, D.V.: 2004, *Astrophys. J.* **605**, 902. DOI.
Colaninno, R.C., Vourlidas, A.: 2015, *Astrophys. J.* **815**, 70. DOI.
Collier, M.R., Lepping, R.P., Berdichevsky, D.B.: 2007, *J. Geophys. Res.* **112**, 06102. DOI.
Dasso, S., Mandrini, C.H., Démoulin, P., Luoni, M.L., Gulisano, A.M.: 2005, *Adv. Space Res.* **35**, 711. DOI.
Dasso, S., Mandrini, C.H., Schmieder, B., Cremades, H., Cid, C., Cerrato, Y., *et al.*: 2009, *J. Geophys. Res.* **114**, 2109. DOI.
Démoulin, P., Bagala, L.G., Mandrini, C.H., Henoux, J.C., Rovira, M.G.: 1997, *Astron. Astrophys.* **325**, 305. ADS
Démoulin, P., Klein, K.L., Goff, C.P., van Driel-Gesztelyi, L., Culhane, J.L., Mandrini, C.H., Matthews, S.A., Harra, L.K.: 2007, *Solar Phys.* **240**, 301. DOI.
Desai, M.I., Mason, G.M., Dwyer, J.R., Mazur, J.E., Gold, R.E., Krimigis, S.M., Smith, C.W., Skoug, R.M.: 2003, *Astrophys. J.* **588**, 1149. DOI.
Desai, M.I., Mason, G.M., Gold, R.E., Krimigis, S.M., Cohen, C.M.S., Mewaldt, R.A., Mazur, J.E., Dwyer, J.R.: 2006, *Astrophys. J.* **649**, 470. DOI.
DeVore, C.R., Antiochos, S.K.: 2008, *Astrophys. J.* **680**, 740. DOI.
Ding, L., Jiang, Y., Zhao, L., Li, G.: 2013, *Astrophys. J.* **763**, 30. DOI.
Ding, L.G., Li, G., Dong, L.H., Jiang, Y., Jian, Y., Gu, B.: 2014a, *J. Geophys. Res.* **119**, 1463. DOI.
Ding, L.G., Li, G., Jiang, Y., Le, G.M., Shen, C.L., Wang, Y.M., Chen, Y., Xu, F., Gu, B., Zhang, Y.N.: 2014b, *Astrophys. J. Lett.* **793**, 35. DOI.
Domingo, V., Fleck, B., Poland, A.I.: 1995, *Solar Phys.* **162**, 1. DOI.
Dresing, N., Gómez-Herrero, R., Klassen, A., Heber, B., Kartavykh, Y., Dröge, W.: 2012, *Solar Phys.* **281**, 281. DOI.
Dryer, M., Steinolfson, R.S., Mihalov, J.D., Wolfe, J.H., Chao, J., Smith, Z.K.: 1976, *J. Geophys. Res.* **81**, 4651. DOI.
Eyles, C.J., Simnett, G.M., Cooke, M.P., Jackson, B.V., Buffington, A., Hick, P.P., *et al.*: 2003, *Solar Phys.* **217**, 319. DOI.
Eyles, C.J., Harrison, R.A., Davis, C.J., Waltham, N.R., Shaughnessy, B.M., Mapson-Menard, H.C.A., *et al.*: 2009, *Solar Phys.* **254**, 387. DOI.
Fan, Y., Gibson, S.E.: 2007, *Astrophys. J.* **668**, 1232. DOI.
Farrugia, C., Berdichevsky, D.: 2004, *Ann. Geophys.* **22**, 3679. DOI.

Farrugia, C.J., Burlaga, L.F., Osherovich, V.A., Richardson, I.G., Freeman, M.P., Lepping, R.P., *et al.*: 1993, *J. Geophys. Res.* **98**, 7621. DOI.
Farrugia, C.J., Jordanova, V.K., Thomsen, M.F., Lu, G., Cowley, S.W.H., Ogilvie, K.W.: 2006a, *J. Geophys. Res.* **111**, A11104. DOI.
Farrugia, C.J., Matsui, H., Kucharek, H., Jordanova, V.K., Torbert, R.B., Ogilvie, K.W., *et al.*: 2006b, *Adv. Space Res.* **38**, 498. DOI.
Forbes, T.G., Priest, E.R.: 1995, *Astrophys. J.* **446**, 377. DOI.
Fritzova-Svestkova, L., Chase, R.C., Svestka, Z.: 1976, *Solar Phys.* **48**, 275. DOI.
Gibson, S.E., Low, B.C.: 1998, *Astrophys. J.* **493**, 460. DOI.
Gonzalez, W.D., Tsurutani, B.T.: 1987, *Planet. Space Sci.* **35**, 1101. DOI.
Gonzalez, W.D., Tsurutani, B.T., Lepping, R.P., Schwenn, R.: 2002, *J. Atmos. Solar-Terr. Phys.* **64**, 173. DOI.
Gopalswamy, N.: 2004, In: Poletto, G., Suess, S.T. (eds.) *The Sun and the Heliosphere as an Integrated System*, *Astrophys. Space. Sci. Lib.* **317**, 201. DOI
Gopalswamy, N.: 2016, *Geosci. Lett.* **3**, 8. DOI.
Gopalswamy, N., Lara, A., Lepping, R.P., Kaiser, M.L., Berdichevsky, D., St. Cyr, O.C.: 2000, *Geophys. Res. Lett.* **27**, 145. DOI.
Gopalswamy, N., Yashiro, S., Kaiser, M.L., Howard, R.A., Bougeret, J.L.: 2001, *Astrophys. J. Lett.* **548**, 91. DOI.
Gopalswamy, N., Yashiro, S., Michałek, G., Kaiser, M.L., Howard, R.A., Reames, D.V., *et al.*: 2002, *Astrophys. J. Lett.* **572**, 103. DOI.
Gopalswamy, N., Aguilar-Rodriguez, E., Yashiro, S., Nunes, S., Kaiser, M.L., Howard, R.A.: 2005, *J. Geophys. Res.* **110**(A9), 12. DOI.
Gopalswamy, N., Yashiro, S., Michalek, G., Stenborg, G., Vourlidas, A., Freeland, S., Howard, R.: 2009, *Earth Moon Planets* **104**, 295. DOI.
Gosling, J.T., Pizzo, V., Bame, S.J.: 1973, *J. Geophys. Res.* **78**, 2001. DOI.
Gosling, J.T., McComas, D.J., Phillips, J.L., Bame, S.J.: 1991, *J. Geophys. Res.* **96**, 7831. DOI.
Gulisano, A.M., Démoulin, P., Dasso, S., Ruiz, M.E., Marsch, E.: 2010, *Astron. Astrophys.* **509**, 39. DOI.
Hansen, R.T., Garcia, C.J., Hansen, S.F., Yasukawa, E.: 1974, *Publ. Astron. Soc. Pac.* **86**, 512. DOI.
Harrison, R.A., Davies, J.A., Rouillard, A.P., Davis, C.J., Eyles, C.J., Bewsher, D., *et al.*: 2009, *Solar Phys.* **256**, 219. DOI.
Harrison, R.A., Davies, J.A., Möstl, C., Liu, Y., Temmer, M., Bisi, M.M., *et al.*: 2012, *Astrophys. J.* **750**, 45. DOI.
Heyvaerts, J., Priest, E.R., Rust, D.M.: 1977, *Astrophys. J.* **216**, 123. DOI
Hill, T.W., Dessler, A.J., Wolf, R.A.: 1976, *Geophys. Res. Lett.* **3**, 429. DOI.
Hillaris, A., Malandraki, O., Klein, K.L., Preka-Papadema, P., Moussas, X., Bouratzis, C., *et al.*: 2011, *Solar Phys.* **273**, 493. DOI.
Hood, A.W., Priest, E.R.: 1979, *Solar Phys.* **64**, 303. DOI.
Hood, A.W., Priest, E.R.: 1980, *Solar Phys.* **66**, 113. DOI.
Hu, Y.Q.: 2001, *Solar Phys.* **200**, 115. DOI.
Hudson, H.S., Bougeret, J.L., Burkepile, J.: 2006, *Space Sci. Rev.* **123**, 13. DOI.
Huttunen, K.E.J., Kilpua, S.P., Pulkkinen, A., Viljanen, A., Tanskanen, E.: 2008, *Space Weather* **6**, 10002. DOI.
Intriligator, D.S.: 1976, *Space Sci. Rev.* **19**, 629. DOI.
Ivanov, K.G.: 1982, *Space Sci. Rev.* **32**, 49. DOI.
Jackson, B.V., Buffington, A., Hick, P.P., Altrock, R.C., Figueroa, S., Holladay, P.E., *et al.*: 2004, *Solar Phys.* **225**, 177. DOI.
Jackson, B.V., Bisi, M.M., Hick, P.P., Buffington, A., Clover, J.M., Sun, W.: 2008, *J. Geophys. Res.* **113**, A00A15. DOI.
Jiang, Y., Shen, Y., Yi, B., Yang, J., Wang, J.: 2008, *Astrophys. J.* **677**, 699. DOI.
Jiang, Y., Yang, J., Hong, J., Bi, Y., Zheng, R.: 2011, *Astrophys. J.* **738**, 179. DOI.
Jin, M., Schrijver, C.J., Cheung, M.C.M., DeRosa, M.L., Nitta, N.V., Title, A.M.: 2016, *Astrophys. J.* **820**, 16. DOI.
Jordanova, V.K., Kistler, L.M., Kozyra, J.U., Khazanov, G.V., Nagy, A.F.: 1996, *J. Geophys. Res.* **101**, 111. DOI.
Jordanova, V.K., Miyoshi, Y.S., Zaharia, S., Thomsen, M.F., Reeves, G.D., Evans, D.S., Mouikis, C.G., Fennell, J.F.: 2006, *J. Geophys. Res.* **111**, 11. DOI.
Joshi, N.C., Uddin, W., Srivastava, A.K., Chandra, R., Gopalswamy, N., Manoharan, P.K., *et al.*: 2013, *Adv. Space Res.* **52**, 1. DOI.
Joshi, N.C., Schmieder, B., Magara, T., Guo, Y., Aulanier, G.: 2016, *Astrophys. J.* **820**, 126. DOI.
Kahler, S.W.: 1992, *Annu. Rev. Astron. Astrophys.* **30**, 113. DOI.
Kahler, S.W.: 2003, *Adv. Space Res.* **32**, 2587. DOI.

Kahler, S.W., Vourlidas, A.: 2005, *J. Geophys. Res.* **110**, 12. DOI.
Kahler, S.W., Vourlidas, A.: 2013, *Astrophys. J.* **769**, 143. DOI.
Kahler, S.W., Vourlidas, A.: 2014, *Astrophys. J.* **784**, 47. DOI.
Kahler, S.W., Arge, C.N., Smith, D.A.: 2016, *Solar Phys.* **291**, 1829. DOI.
Kahler, S.W., Reames, D.V., Sheeley, N.R. Jr.: 2001, *Astrophys. J.* **562**, 558. DOI.
Kahler, S.W., Sheeley, N.R., Howard, R.A., Michels, D.J., Koomen, M.J., McGuire, R.E., von Rosenvinge, T.T., Reames, D.V.: 1984, *J. Geophys. Res.* **89**, 9683. DOI
Kaiser, M.L., Kucera, T.A., Davila, J.M., St. Cyr, O.C., Guhathakurta, M., Christian, E.: 2008, *Space Sci. Rev.* **136**, 5. DOI.
Kallenrode, M.B.: 2001 In: *Proc. 27th ICRC 8*, 3273. ADS
Kallenrode, M.B., Wibberenz, G., Kunow, H., Müller-Mellin, R., Stolpovskii, V., Kontor, N.: 1993, *Solar Phys.* **147**, 377. DOI.
Kamide, Y., Yokoyama, N., Gonzalez, W., Tsurutani, B.T., Daglis, I.A., Brekke, A., Masuda, S.: 1998, *J. Geophys. Res.* **103**, 6917. DOI.
Klein, K.L.: 2006, In: Gopalswamy, N., Mewaldt, R., Torsti, J. (eds.) *Solar Eruptions and Energetic Particles*, *AGU Geophys. Monogr.* **165**, 233. DOI
Klein, K.L., Krucker, S., Lointier, G., Kerdraon, A.: 2008, *Astron. Astrophys.* **486**, 589. DOI.
Kliem, B., Török, T.: 2006, *Phys. Rev. Lett.* **96**, 255002. DOI.
Kliem, B., MacKinnon, A., Trottet, G., *et al.*: 2003, In: Klein, L. (ed.) *Energy Conversion and Particle Acceleration in the Solar Corona*, *Lec. Notes Phys.* **612**, 263. ADS
Krucker, S., Larson, D.E., Lin, R.P., Thompson, B.J.: 1999, *Astrophys. J.* **519**, 864. DOI.
Kusano, K., Maeshiro, T., Yokoyama, T., Sakurai, T.: 2004, *Astrophys. J.* **610**, 537. DOI.
le Roux, J.A., Fichtner, H.: 1999, *J. Geophys. Res.* **104**, 4709. DOI.
Li, G., Zank, G.P.: 2005 In: *Proc. 29th ICRC*, 173. ADS
Li, L.P., Zhang, J.: 2013, *Astron. Astrophys.* **552**, 11. DOI.
Li, G., Moore, R., Mewaldt, R.A., Zhao, L., Labrador, A.W.: 2012, *Space Sci. Rev.* **171**, 141. DOI.
Lin, J., Forbes, T.G.: 2000, *J. Geophys. Res.* **105**, 2375. DOI.
Lin, R.P., Hudson, H.S.: 1976, *Solar Phys.* **50**, 153. DOI.
Liu, Y.D., Luhmann, J.G., Möstl, C., Martinez-Oliveros, J.C., Bale, S.D., Lin, R.P., *et al.*: 2012, *Astrophys. J. Lett.* **746**, 15. DOI.
Liu, Y.D., Luhmann, J.G., Lugaz, N., Möstl, C., Davies, J.A., Bale, S.D., *et al.*: 2013, *Astrophys. J.* **769**, 45. DOI.
Liu, Y.D., Luhmann, J.G., Kajdič, P., Kilpua, E.K.J., Lugaz, N., Nitta, N.V., *et al.*: 2014a, *Nat. Commun.* **5**, 3481. DOI.
Liu, Y.D., Yang, Z., Wang, R., Luhmann, J.G., Richardson, J.D., Lugaz, N.: 2014b, *Astrophys. J. Lett.* **793**, 41. DOI.
Liu, Y.D., Hu, H., Wang, R., Yang, Z., Zhu, B., Liu, Y.A., *et al.*: 2015, *Astrophys. J. Lett.* **809**, 34. DOI.
Lopez, R.E.: 1987, *J. Geophys. Res.* **92**, 11189. DOI.
Lugaz, N., Farrugia, C.J.: 2014, *Geophys. Res. Lett.* **41**, 769. DOI.
Lugaz, N., Manchester, W.B., Gombosi, T.I.: 2005, *Astrophys. J.* **634**, 651. DOI.
Lugaz, N., Vourlidas, A., Roussev, I.I.: 2009, *Ann. Geophys.* **27**, 3479. DOI.
Lugaz, N., Manchester, W.B., Roussev, I.I., Tóth, G., Gombosi, T.I.: 2007, *Astrophys. J.* **659**, 788. DOI.
Lugaz, N., Vourlidas, A., Roussev, I.I., Jacobs, C., Manchester, W.B. IV, Cohen, O.: 2008, *Astrophys. J. Lett.* **684**, 111. DOI.
Lugaz, N., Vourlidas, A., Roussev, I.I., Morgan, H.: 2009, *Solar Phys.* **256**, 269. DOI.
Lugaz, N., Farrugia, C.J., Davies, J.A., Möstl, C., Davis, C.J., Roussev, I.I., Temmer, M.: 2012, *Astrophys. J.* **759**, 68. DOI.
Lugaz, N., Farrugia, C.J., Manchester, W.B., Schwadron, N.: 2013, *Astrophys. J.* **778**, 20. DOI.
Lugaz, N., Farrugia, C.J., Huang, C.L., Spence, H.E.: 2015a, *Geophys. Res. Lett.* **42**, 4694. DOI.
Lugaz, N., Farrugia, C.J., Smith, C.W., Paulson, K.: 2015b, *J. Geophys. Res.* **120**, 2409. DOI.
Lugaz, N., Farrugia, C.J., Winslow, R.M., Al-Haddad, N., Kilpua, E.K.J., Riley, P.: 2016, *J. Geophys. Res.* **121**, 10861. DOI.
Luhmann, J.G., Ledvina, S.A., Odstrcil, D., Owens, M.J., Zhao, X.P., Liu, Y., Riley, P.: 2010, *Adv. Space Res.* **46**, 1. DOI.
Lynch, B.J., Edmondson, J.K.: 2013, *Astrophys. J.* **764**, 87. DOI.
Lyons, M.A., Simnett, G.M.: 1999, *Solar Phys.* **186**, 363. DOI.
MacDowall, R.J.: 1989, *Geophys. Res. Lett.* **16**, 923. DOI.
MacTaggart, D., Hood, A.W.: 2009, *Astron. Astrophys.* **508**, 445. DOI.
Malandraki, O.E., Marsden, R.G., Lario, D., Tranquille, C., Heber, B., Mewaldt, R.A., *et al.*: 2009, *Astrophys. J.* **704**, 469. DOI.
Manchester, W.: 2003, *J. Geophys. Res.* **108**, 1162. DOI.

Mann, G., Classen, T., Aurass, H.: 1995, *Astron. Astrophys.* **295**, 775. ADS
Maričić, D., Vršnak, B., Dumbović, M., Žic, T., Roša, D., Hržina, D., *et al.*: 2014, *Solar Phys.* **289**, 351. DOI.
Martínez Oliveros, J.C., Raftery, C.L., Bain, H.M., Liu, Y., Krupar, V., Bale, S., *et al.*: 2012, *Astrophys. J.* **748**, 66. DOI.
Mason, G.M., Mazur, J.E., Dwyer, J.R.: 1999, *Astrophys. J. Lett.* **525**, 133. DOI.
Masson, S., Antiochos, S.K., DeVore, C.R.: 2013, *Astrophys. J.* **771**, 82. DOI.
Masson, S., Démoulin, P., Dasso, S., Klein, K.L.: 2012, *Astron. Astrophys.* **538**, 32. DOI.
Mishra, W., Srivastava, N., Chakrabarty, D.: 2015, *Solar Phys.* **290**, 527. DOI.
Mishra, W., Srivastava, N., Singh, T.: 2015, *J. Geophys. Res.* **120**, 10. DOI.
Mishra, W., Wang, Y., Srivastava, N.: 2016, *Astrophys. J.* **831**, 99. DOI.
Miteva, R., Klein, K.L., Kienreich, I., Temmer, M., Veronig, A., Malandraki, O.E.: 2014, *Solar Phys.* **289**, 2601. DOI.
Miyoshi, Y., Kataoka, R.: 2005, *Geophys. Res. Lett.* **32**, 21105. DOI.
Moon, Y.J., Choe, G.S., Wang, H., Park, Y.D., Gopalswamy, N., Yang, G., *et al.*: 2002, *Astrophys. J.* **581**, 694. DOI.
Moon, Y.J., Chae, J., Wang, H., Park, Y.D.: 2003a, *Adv. Space Res.* **32**, 1953. DOI.
Moon, Y.J., Choe, G.S., Wang, H., Park, Y.D.: 2003b, *Astrophys. J.* **588**, 1176. DOI.
Moore, R.L., Sterling, A.C., Hudson, H.S., Lemen, J.R.: 2001, *Astrophys. J.* **552**, 833. DOI.
Möstl, C., Farrugia, C.J., Kilpua, E.K.J., Jian, L.K., Liu, Y., Eastwood, J.P., *et al.*: 2012, *Astrophys. J.* **758**, 10. DOI.
Mühlbachler, S., Farrugia, C.J., Raeder, J., Biernat, H.K., Torbert, R.B.: 2005, *J. Geophys. Res.* **110**, 11207. DOI.
Nieves-Chinchilla, T., Colaninno, R., Vourlidas, A., Szabo, A., Lepping, R.P., Boardsen, S.A., *et al.*: 2012, *J. Geophys. Res.* **117**, 6106. DOI.
Nitta, N.V., Hudson, H.S.: 2001, *Geophys. Res. Lett.* **28**, 3801. DOI.
Odstrcil, D., Pizzo, V.J.: 2009, *Solar Phys.* **259**, 297. DOI.
Odstrcil, D., Vandas, M., Pizzo, V.J., MacNeice, P.: 2003, In: Velli, M., Bruno, R., Malara, F., Bucci, B. (eds.) *Solar Wind Ten*, *Amer. Inst. Physics Conf. Ser.* **679**, 699. DOI.
Owens, M.J., Crooker, N.U.: 2006, *J. Geophys. Res.* **111**, A10104. DOI.
Pearce, G., Harrison, R.A.: 1990, *Astron. Astrophys.* **228**, 513. ADS
Pesnell, W.D., Thompson, B.J., Chamberlin, P.C.: 2012, *Solar Phys.* **275**, 3. DOI.
Pevtsov, A.A.: 2000, *Astrophys. J.* **531**, 553. DOI.
Poedts, S., van der Holst, B., Chattopadhyay, I., Banerjee, D., van Lier, T., Keppens, R.: 2003, In: Wilson, A. (ed.) *Solar Variability as an Input to the Earth's Environment*, *ESA* **SP-535**, 603. ADS
Poomvises, W., Zhang, J., Olmedo, O.: 2010, *Astrophys. J. Lett.* **717**, 159. DOI.
Prise, A.J., Harra, L.K., Matthews, S.A., Arridge, C.S., Achilleos, N.: 2015, *J. Geophys. Res.* **120**, 1566. DOI.
Qiu, J., Hu, Q., Howard, T.A., Yurchyshyn, V.B.: 2007, *Astrophys. J.* **659**, 758. DOI.
Reames, D.V.: 1990, *Astrophys. J. Suppl. Ser.* **73**, 235. DOI.
Reames, D.V.: 1999, *Space Sci. Rev.* **90**, 413. DOI.
Reames, D.V.: 2013, *Space Sci. Rev.* **175**, 53. DOI.
Reiner, M.J., Kaiser, M.L.: 1999, *Geophys. Res. Lett.* **26**, 397. DOI.
Reiner, M.J., Kaiser, M.L., Bougeret, J.L.: 2001, *J. Geophys. Res.* **106**, 29989. DOI.
Reiner, M.J., Vourlidas, A., St. Cyr, O.C., Burkepile, J.T., Howard, R.A., Kaiser, M.L., *et al.*: 2003, *Astrophys. J.* **590**, 533. DOI.
Richardson, R.S.: 1951, *Astrophys. J.* **114**, 356. DOI
Richardson, I.G., Cane, H.V.: 1993, *J. Geophys. Res.* **98**, 15. DOI.
Richardson, I.G., Cane, H.V.: 1995, *J. Geophys. Res.* **100**, 23397. DOI.
Richardson, I.G., Cane, H.V.: 2010a, *J. Geophys. Res.* **115**, 7103. DOI.
Richardson, I.G., Cane, H.V.: 2010b, *Solar Phys.* **264**, 189. DOI.
Richardson, I.G., Zhang, J.: 2008, *Geophys. Res. Lett.* **35**, 6. DOI.
Richardson, I.G., Cane, H.V., von Rosenvinge, T.T.: 1991, *J. Geophys. Res.* **96**, 7853. DOI.
Richardson, I.G., Lawrence, G.R., Haggerty, D.K., Kucera, T.A., Szabo, A.: 2003, *Geophys. Res. Lett.* **30**, 2. DOI.
Rodríguez-Gasén, R., Aran, A., Sanahuja, B., Jacobs, C., Poedts, S.: 2014, *Solar Phys.* **289**, 1745. DOI.
Rouillard, A.P., Sheeley, N.R., Tylka, A., Vourlidas, A., Ng, C.K., Rakowski, C., *et al.*: 2012, *Astrophys. J.* **752**, 44. DOI.
Ruffolo, D., Tooprakai, P., Rujiwarodom, M., Khumlumlert, T., Wechakama, M., Bieber, J.W., *et al.*: 2006, *Astrophys. J.* **639**, 1186. DOI.
Sanderson, T.R., Marsden, R.G., Heras, A.M., Wenzel, K.P., Anglin, J.D., Balogh, A., Forsyth, R.: 1992, *Geophys. Res. Lett.* **19**, 1263. DOI.

Savani, N.P., Rouillard, A.P., Davies, J.A., Owens, M.J., Forsyth, R.J., Davis, C.J., *et al.*: 2009, *Ann. Geophys.* **27**, 4349. DOI.
Schmidt, J., Cargill, P.: 2004, *Ann. Geophys.* **22**, 2245. DOI.
Schmieder, B., Simon, G., Martres, M.J., Mein, P., Mein, N., Tandberg-Hanssen, E.: 1984, *Adv. Space Res.* **4**, 27. DOI.
Schrijver, C.J., Title, A.M.: 2011, *J. Geophys. Res.* **116**, 04108. DOI.
Schrijver, C.J., Aulanier, G., Title, A.M., Pariat, E., Delannée, C.: 2011, *Astrophys. J.* **738**, 167. DOI.
Schrijver, C.J., Title, A.M., Yeates, A.R., DeRosa, M.L.: 2013, *Astrophys. J.* **773**, 93. DOI.
Schwadron, N.A., Connick, D.E., Smith, C.: 2010, *Astrophys. J. Lett.* **722**, 132. DOI.
Schwenn, R.: 2006, *Living Rev. Solar Phys.* **3**, 2. DOI.
Shen, Y., Liu, Y., Su, J.: 2012, *Astrophys. J.* **750**, 12. DOI.
Shen, F., Feng, X.S., Wang, Y., Wu, S.T., Song, W.B., Guo, J.P., *et al.*: 2011, *J. Geophys. Res.* **116**, 9103. DOI.
Shen, C., Wang, Y., Wang, S., Liu, Y., Liu, R., Vourlidas, A., *et al.*: 2012a, *Nat. Phys.* **8**, 923. DOI.
Shen, F., Wu, S.T., Feng, X.S., Wu, C.C.: 2012b, *J. Geophys. Res.* **117**, 11101. DOI.
Shen, C., Li, G., Kong, X., Hu, J., Sun, X.D., Ding, L., *et al.*: 2013a, *Astrophys. J.* **763**, 114. DOI.
Shen, C., Liao, C., Wang, Y., Ye, P., Wang, S.: 2013b, *Solar Phys.* **282**, 543. DOI.
Shen, F., Shen, C., Wang, Y., Feng, X., Xiang, C.: 2013c, *Geophys. Res. Lett.* **40**, 1457. DOI.
Shen, F., Wang, Y., Shen, C., Feng, X.: 2016, *Sci. Rep.* **6**, 19576. DOI.
Shen, F., Wang, Y., Shen, C., Feng, X.: 2017, *Solar Phys.*, submitted. SOLA-D-16-00199
Shue, J.-H., Song, P., Russell, C.T., Steinberg, J.T., Chao, J., Zastenker, G., *et al.*: 1998, *J. Geophys. Res.* **103**, 17691. DOI.
Simnett, G.M., Hudson, H.S.: 1997, Correlated phenomena at the Sun, in the heliosphere and in geospace. In: *Proc. 31st ESLAB Symp.*, *ESA* **SP-415**, 437. ADS
Siscoe, G.L., Crooker, N.U., Siebert, K.D.: 2002, *J. Geophys. Res.* **107**, 1321. DOI.
Siscoe, G.L., McPherron, R.L., Jordanova, V.K.: 2005, *J. Geophys. Res.* **110**, 12227. DOI.
Soenen, A., Zuccarello, F.P., Jacobs, C., Poedts, S., Keppens, R., van der Holst, B.: 2009, *Astron. Astrophys.* **501**, 1123. DOI.
Sokolov, I.V., Roussev, I.I., Fisk, L.A., Lee, M.A., Gombosi, T.I., Sakai, J.I.: 2006, *Astrophys. J. Lett.* **642**, 81. DOI.
Steinolfson, R.S.: 1982, *Astron. Astrophys.* **115**, 50. ADS
Sterling, A.C., Moore, R.L.: 2001, *Astrophys. J.* **560**, 1045. DOI.
Sterling, A.C., Moore, R.L., Falconer, D.A., Knox, J.M.: 2014, *Astrophys. J. Lett.* **788**, 20. DOI.
Sun, X., Hoeksema, J.T., Liu, Y., Wiegelmann, T., Hayashi, K., Chen, Q., *et al.*: 2012, *Astrophys. J.* **748**, 77. DOI.
Svestka, Z.F., Jackson, B.V., Howard, R.A., Sheeley, N.R. Jr.: 1989, *Solar Phys.* **122**, 131. DOI.
Temmer, M., Nitta, N.V.: 2015, *Solar Phys.* **290**, 919. DOI.
Temmer, M., Rollett, T., Möstl, C., Veronig, A.M., Vršnak, B., Odstrčil, D.: 2011, *Astrophys. J.* **743**, 101. DOI.
Temmer, M., Vršnak, B., Rollett, T., Bein, B., de Koning, C.A., Liu, Y., *et al.*: 2012, *Astrophys. J.* **749**, 57. DOI.
Temmer, M., Veronig, A.M., Peinhart, V., Vršnak, B.: 2014, *Astrophys. J.* **785**, 85. DOI.
Thernisien, A.: 2011, *Astrophys. J. Suppl. Ser.* **194**, 33. DOI.
Titov, V.S., Démoulin, P.: 1999, *Astron. Astrophys.* **351**, 707. ADS
Titov, V.S., Mikic, Z., Török, T., Linker, J.A., Panasenco, O.: 2012, *Astrophys. J.* **759**, 70. DOI.
Török, T., Kliem, B.: 2003, *Astron. Astrophys.* **406**, 1043. DOI.
Török, T., Kliem, B., Titov, V.S.: 2004, *Astron. Astrophys.* **413**, 27. DOI.
Török, T., Panasenco, O., Titov, V.S., Mikić, Z., Reeves, K.K., Velli, M., *et al.*: 2011, *Astrophys. J.* **739**, 63. DOI.
Tóth, G., Sokolov, I.V., Gombosi, T.I., Chesney, D.R., Clauer, C.R., De Zeeuw, D.L., *et al.*: 2005, *J. Geophys. Res.* **110**, A12226. DOI.
Tóth, G., De Zeeuw, D.L., Gombosi, T.I., Manchester, W.B., Ridley, A.J., Sokolov, I.V., *et al.*: 2007, *Space Weather* **5**, 06003. DOI.
Tóth, G., van der Holst, B., Sokolov, I.V., De Zeeuw, D.L., Gombosi, T.I., Fang, F., *et al.*: 2012, *J. Comput. Phys.* **231**, 870. DOI.
Tsurutani, B.T., Smith, E.J., Gonzalez, W.D., Tang, F., Akasofu, S.I.: 1988, *J. Geophys. Res.* **93**, 8519. DOI.
Tsurutani, B.T., Gonzalez, W.D.: 1997, In: Tsurutani, B.T., *et al.* (eds.) *Magnetic Storms*, *AGU Geophys. Monogr.* **98**, 77. DOI.
Tsurutani, B.T., Hajra, R., Echer, E., Gjerloev, J.W.: 2015, *Ann. Geophys.* **33**, 519. DOI.
Tylka, A.J., Cohen, C.M.S., Dietrich, W.F., Lee, M.A., Maclennan, C.G., Mewaldt, R.A., *et al.*: 2005, *Astrophys. J.* **625**, 474. DOI.

Usoskin, I.G.: 2013, *Living Rev. Solar Phys.* **10**, 1. DOI.
van der Holst, B., Sokolov, I.V., Meng, X., Jin, M., Manchester, W.B., Tóth, G., *et al.*: 2014, *Astrophys. J.* **782**, 81. DOI.
Vandas, M., Fischer, S., Dryer, M., Smith, Z., Detman, T., Geranios, A.: 1997, *J. Geophys. Res.* **102**, 22295. DOI.
Vasyliūnas, V.M.: 2004, *Adv. Space Res.* **33**, 2113. DOI.
Vemareddy, P., Ambastha, A., Maurya, R.A.: 2012, *Astrophys. J.* **761**, 60. DOI.
Vourlidas, A., Subramanian, P., Dere, K.P., Howard, R.A.: 2000, *Astrophys. J.* **534**, 456. DOI.
Vršnak, B.: 2001, *Solar Phys.* **202**, 173. DOI.
Wang, Y.M., Sheeley, N.R. Jr.: 1990, *Astrophys. J.* **355**, 726. DOI.
Wang, Y.M., Wang, S., Ye, P.Z.: 2002, *Solar Phys.* **211**, 333. DOI.
Wang, Y.M., Ye, P.Z., Wang, S.: 2003, *J. Geophys. Res.* **108**, 6. DOI.
Wang, H., Chae, J., Yurchyshyn, V., Yang, G., Steinegger, M., Goode, P.: 2001, *Astrophys. J.* **559**, 1171. DOI.
Wang, Y.M., Ye, P.Z., Wang, S., Xue, X.H.: 2003a, *Geophys. Res. Lett.* **30**, 33. DOI.
Wang, Y.M., Ye, P.Z., Wang, S., Xiong, M.: 2003b, *Solar Phys.* **216**, 295. DOI.
Wang, Y., Shen, C.L., Wang, S., Ye, P.Z.: 2003c, *Geophys. Res. Lett.* **30**, 2039. DOI.
Wang, Y.M., Zheng, H., Wang, S., Ye, P.: 2005, *Astron. Astrophys.* **434**, 309. DOI.
Wang, Y., Chen, C., Gui, B., Shen, C., Ye, P., Wang, S.: 2011, *J. Geophys. Res.* **116**, 04104. DOI.
Wang, S., Liu, C., Liu, R., Deng, N., Liu, Y., Wang, H.: 2012, *Astrophys. J. Lett.* **745**, 17. DOI.
Wang, Y., Liu, L., Shen, C., Liu, R., Ye, P., Wang, S.: 2013, *Astrophys. J. Lett.* **763**, 43. DOI.
Wang, R., Liu, Y.D., Yang, Z., Hu, H.: 2014a, *Astrophys. J.* **791**, 84. DOI.
Wang, Y., Wang, B., Shen, C., Shen, F., Lugaz, N.: 2014b, *J. Geophys. Res.* **119**, 5117. DOI.
Wang, Y., Zhou, Z., Shen, C., Liu, R., Wang, S.: 2015, *J. Geophys. Res.* **120**, 1543. DOI.
Wang, R., Liu, Y.D., Zimovets, I., Hu, H., Dai, X., Yang, Z.: 2016, *Astrophys. J. Lett.* **827**, 12. DOI.
Webb, D.F., Kahler, S.W., McIntosh, P.S., Klimchuck, J.A.: 1997, *J. Geophys. Res.* **102**, 24161. DOI.
Webb, D.F., Cliver, E.W., Crooker, N.U., Cry, O.C.S., Thompson, B.J.: 2000, *J. Geophys. Res.* **105**, 7491. DOI.
Webb, D.F., Howard, T.A., Fry, C.D., Kuchar, T.A., Odstrcil, D., Jackson, B.V., *et al.*: 2009, *Solar Phys.* **256**, 239. DOI.
Wheatland, M.S.: 2000, *Astrophys. J.* **536**, 109. DOI.
Wiegelmann, T., Thalmann, J.K., Inhester, B., Tadesse, T., Sun, X., Hoeksema, J.T.: 2012, *Solar Phys.* **281**, 37. DOI.
Winslow, R.M., Lugaz, N., Schwadron, N.A., Farrugia, C.J., Yu, W., Raines, J.M., *et al.*: 2016, *J. Geophys. Res.* **121**, 6092. DOI.
Wu, S.T., Wang, A.H., Gopalswamy, N.: 2002. In: *Proceedings of the Magnetic Coupling of the Solar Atmosphere Euroconference, SOLMAG 2002*, *ESA* **SP-505**, 227. ADS
Wu, C.C., Liou, K., Vourlidas, A., Plunkett, S., Dryer, M., Wu, S.T., *et al.*: 2016, *J. Geophys. Res.* **121**, 1839. DOI.
Xie, H., Gopalswamy, N., Manoharan, P.K., Lara, A., Yashiro, S., Lepri, S.: 2006, *J. Geophys. Res.* **111**, 1103. DOI.
Xiong, M., Zheng, H., Wang, S.: 2009, *J. Geophys. Res.* **114**, 11101. DOI.
Xiong, M., Zheng, H., Wang, Y., Wang, S.: 2006, *J. Geophys. Res.* **111**, A08105. DOI.
Xiong, M., Zheng, H., Wu, S.T., Wang, Y., Wang, S.: 2007, *J. Geophys. Res.* **112**, 11103. DOI.
Yang, J., Jiang, Y., Zheng, R., Bi, Y., Hong, J., Yang, B.: 2012, *Astrophys. J.* **745**, 9. DOI.
Yashiro, S., Michalek, G., Gopalswamy, N.: 2008, *Ann. Geophys.* **26**, 3103. DOI.
Yashiro, S., Gopalswamy, N., Michalek, G., St. Cyr, O.C., Plunkett, S.P., Rich, N.B., Howard, R.A.: 2004, *J. Geophys. Res.* **109**, 07105. DOI.
Zank, G.P., Rice, W.K.M., Wu, C.C.: 2000, *J. Geophys. Res.* **105**, 25079. DOI.
Zhang, J., Wang, J.: 2002, *Astrophys. J.* **566**, 117. DOI.
Zhang, Y., Liu, J., Zhang, H.: 2008, *Solar Phys.* **247**, 39. DOI.
Zhang, J., Richardson, I.G., Webb, D.F.: 2008, *J. Geophys. Res.* **113**, 00. DOI.
Zhang, J., Richardson, I.G., Webb, D.F., Gopalswamy, N., Huttunen, E., Kasper, J.C., *et al.*: 2007, *J. Geophys. Res.* **112**, A10102. DOI.